UNIVERSITY OF CALIFORNIA, SAN DIEGO

Sliding-layer laminates: a new robotic material enabling robust and adaptable undulatory locomotion

A Thesis submitted in partial satisfaction of the
requirements for the degree Master of Science

in

Engineering Sciences (Mechanical Engineering)

by

Mingsong Jiang

Committee in charge:

Professor Nicholas Gravish, Chair
Professor Michael Tolley
Professor Michael Yip

2018

The Thesis of Mingsong Jiang is approved and it is acceptable in quality and form for publication on microfilm and electronically.

_____

_____

_____

Chair

University of California, San Diego

2018

TABLE OF CONTENTS

LIST OF FIGURES

LIST OF TABLES

ACKNOWLEDGEMENTS

My stay at the University of California San Diego has been an exciting and research life defining experience that would not have been possible without the support of colleagues, and my advisor. I have benefited from their creativity and insights and take away a very important lesson that can only truly be appreciated through experience; research requires resilience.

There are many people to thank, I would begin with my first thank to my advisor Prof. Nicholas G. Gravish for his unceasingly inspiring instructions during my research. The project of the Sliding Layered Laminate is motivated by his creative thoughts and further achieved under his guidance. Each single experiment is well planned in such a logical way, especially for exploring a new research concept such as a variable stiffness SLL design, to prove the usefulness of an innovative scientific idea. Without him I cannot finish this innovative material designs in such a short time.

A sincere thankfulness to Prof. Michael T. Tolley for his great supports in my experimental prototyping for the SLL. Without the laser system in his lab, the fabrication of a SLL would be delayed with a lack of accuracy for material cuts. In the same time, I want to thank all the lab members from BRDL, Aaron, William, Caleb, Dylan, Daniel, Adriane, Saurabh and all the others for their great help in training me the use of the laser system and other scientific tools and devices extremely accelerating my research paces.

I want to thank Prof. Yip for his attending of my final thesis defense and give me precious advices.

In the end, I want to thank all my lab members, Glenna, Dennis, Shivam, Steve, Daniel, Wei and all the other members who have to some extent involved get helped me with all kinds of

challenges and difficulties during my research and the constructive suggestions they have ever made in help me achieving my research progress.

ABSTRACT OF THE THESIS

Sliding-layer laminates: a new robotic material enabling robust and adaptable undulatory locomotion

by

Mingsong Jiang

Master of Science in Engineering Sciences (Mechanical Engineering)

University of California, San Diego, 2018

Dr. Nicholas G. Gravish, Chair

New robotic devices will benefit from new materials capable of controllable and variable material properties. In this thesis, we present a new composite laminated material with periodically arranged patterns of stiff and soft regions, laminated together in a multi-layer configuration with a central sliding layer, which is called sliding-layer laminates (SLLs). We first build a model based on Euler-Bernoulli beam theory and compute the stiffness variation as a function of layer alignment; we then explore the design principles, manipulating the stiffness patterning on the SLLs using computational and experimental methods. The comparison theory and experiment for two

design principles exhibited strong agreement with differences only in the soft SLLs. In experiment, we demonstrate an up to 6-7 folds stiffness variation based on the fixed end cantilever beam test and an infinite stiffness variation is observed from the theoretical model. The effective bending stiffness under different sliding positions of the central laminate varies continuously with sufficiently many intermediate stiffness states available. To demonstrate the applicability of SLLs for robot locomotion, we implemented our SLL as a variable compliance wing structure in a wind tunnel and a robotic fish tail in a water tank to observe both the fluttering (air flow) and flapping motions (water flow) under actively tunable stiffness. The result shows great changes in amplitude (wing tip) and force (tail body) generations which indicates strong applications for multi-functional material to be exploited in mobile robots to achieve high performance under changing working conditions. In the future we envision, that SLL can be further extended into multiple areas, including innovative fabrication methods, multi-convertible properties, and high-dimensioned structures which will promote low-cost, easy controlled variable compliance solution into more unknown fields. Representative of a whole type of smart materials with tunable physical properties, the development of the SLL is still in its infancy, and the future applications of such an integrated multi-functionality system can be broadly extended in assisting the construction of bio-inspired Robotics.

Keywords: variable compliance, stiffness, laminate, robotics

Chapter 1.

Introduction

In general, deformation of a system is primarily characterized by its mechanical compliance. Mechanical compliance is the reciprocal of stiffness and is defined as the measure of the ability of a structure to exhibit a deformation due to the action of external forces. It is essential in robotic structural design considering both safe human-machine interactions as well as modulating other physical properties, such as force and speed. Traditional robots are mainly assembled by rigid materials and structures with fixed geometry structural elements. To improve the usability of future robots in different many scenarios, a variable compliance structure/mechanism should be considered [1]. A Variable compliant mechanism is a novel multi-functionality to selectively modulate the compliance of a system depending on operating requirements or working environments (figure 1.1). As future robots are poised to serve under changing and more complex work environments, variable compliance can help improve the functionality of a system under certain operating condition. This chapter introduces the importance of variable compliance in current robotic designs, followed by current technologies in achieving variable compliance exploring different mechanisms and the advantages of using laminating process and laser cutting technology in achieving low-profile variable compliance materials,

named as Sliding Layered Laminates (SLLs), as building blocks or dynamic appendages for future robotics.

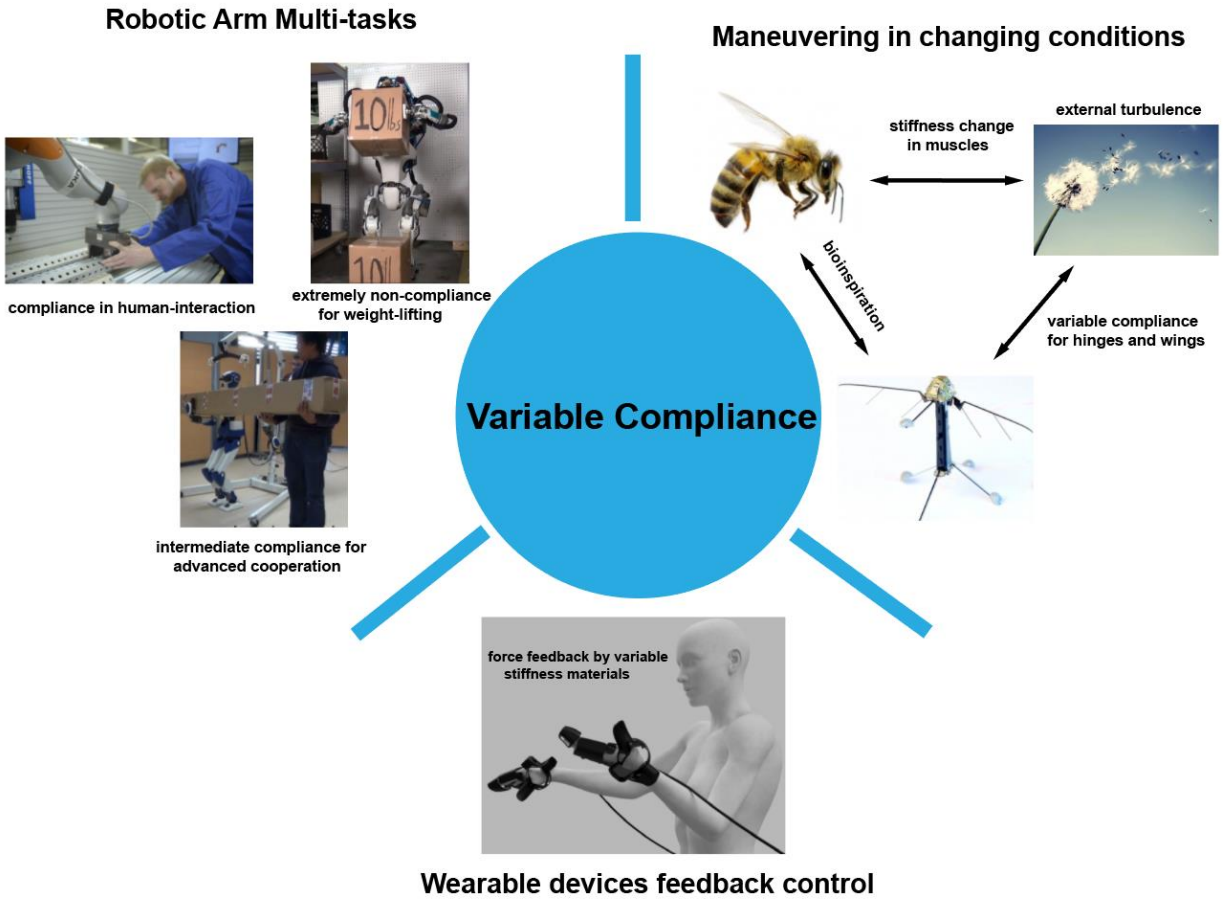

Figure 1.1 An overall showcase of variable compliance general applications in robotic designs.

1.1 Variable compliance in robotic designs

Nowadays, a big challenge facing current service robots is its conventional constrained design principles where rigid body metal frame is commonly used and the compliance of either the execution part or the whole body or part of the appendage maintains a constant. Such a feature offers only acceptable performances over a range of operating conditions, however cannot be optimized under variable work environments [2]. To solve this, a structure with active modulation

of variable compliance will be favorable in achieving robot's multi-functionalities and to negotiate with changing operating conditions.

1.1.1 Variable compliance in mobile robots

Variable compliance as a novel design principle can be applied into many current robotic designs. In mobile robots, such a property can be embedded as a building block for appendages of robots. For instance, RHex is an autonomous legged robot aiming at unmanned explorations and rescue [3-5]. Its energy efficiency is highly dependent on the COM (Center of Mass) trajectory which is intermediately determined by the legged stiffness as a compliant interaction with the ground surface [6-8]. Based on this, researchers have developed variable stiffness C-leg (figure 1.2) as to provide both energy efficiency and flexibilities in dealing with changing environments. In theoretical SLIP (Spring Loaded Inverted Pendulum) modelling, a physically variable stiffness actuator has been proved successful in modulating both spring force over a wide range of bandwidth that showed great consistence with an ideal SLIP model compared with non-variable spring stiffness actuators [6]. It reveals a practical solution in realizing highly dynamic locomotion by adding variable compliance to a system. In the meanwhile, variable stiffness of fish body is proved to be capable of modulating swimming performance such as propelling force and swimming speeds which indicates strong applications of variable compliance fish appendages such as fins and pedals for robust swimming robots [9-11], shown in figure 1.3.

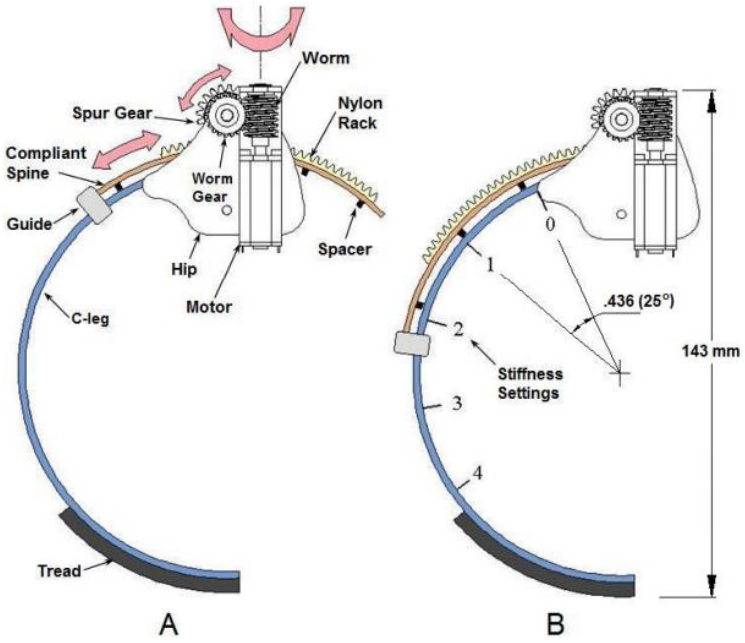

Figure 1.2: Side view of a tunable stiffness composite C-leg design [1].

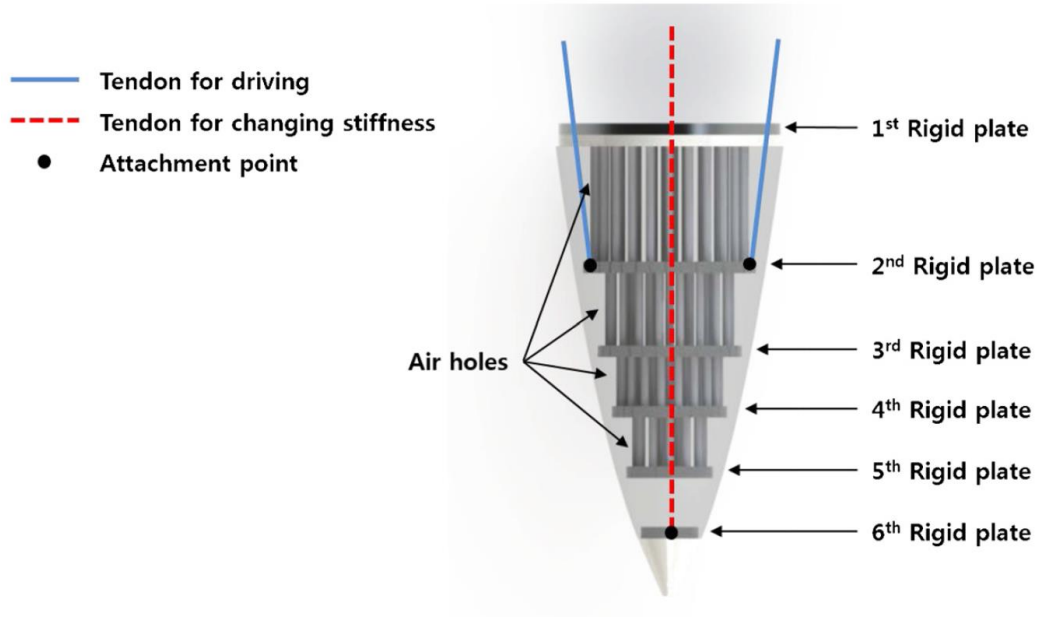

Figure 1.3: Design of a robotic tail's driving part with variable-stiffness structure and tendons (red dashed line: tendon for changing stiffness, blue solid lines: tendons for driving, dots: attachment points) [7].

1.1.2 Variable compliance in soft robots

A new trend in robotics is building robots using soft materials as a means to contend with the limitations of service robots in negotiating with natural environments. The inherent softness of the compliant materials enables safe interactions with surroundings [12]; however, with variable compliance or stiffening effects, the output force generated by the structural interface can be modulated or increased when necessary. For example, soft robotic grippers exploiting jamming effects from granular materials are capable of both compliant interactions in the off-state (no evacuation of air) and highly increased grasping force in the on-state (with air evacuated) [13] as shown in figure 1.4. The variable compliance actuated by the change of relative distances between each granular particle help to provide secured gripping performances than traditional fingered type mechanical grippers especially on irregular, undetermined shapes of targets [14]. On the other hand, self-folding origamis implanted with variable compliance laminates can be improved to achieved different folding angles with the same heat input and thus could be cooperate with heat control for the optimized energy efficiency [15][16], shown in figure 1.5.

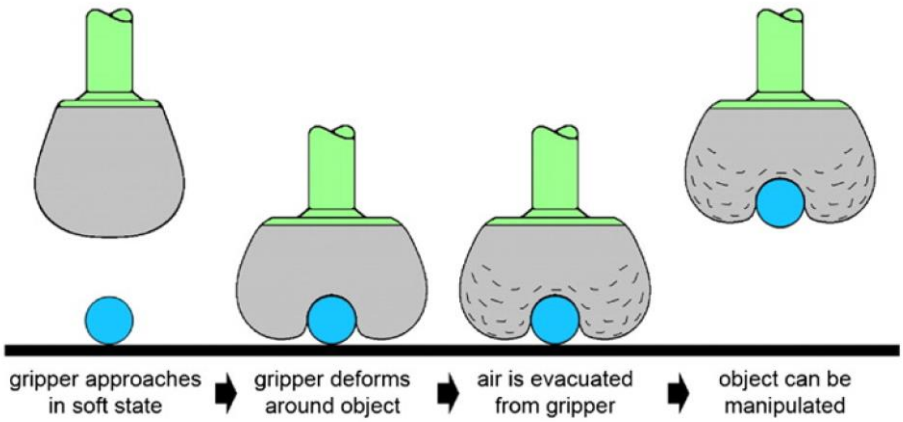

Figure 1.4 Schematics of jamming grippers in achieving both soft interactions and stiffened gripping performances [9].

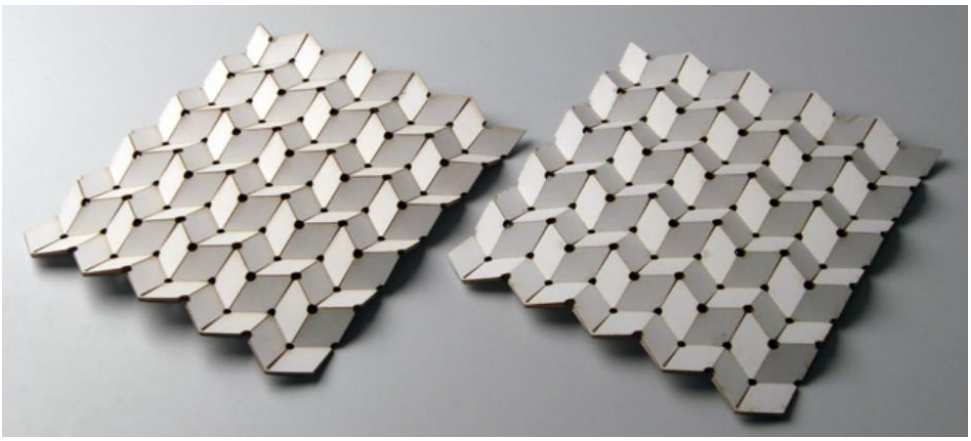

Figure 1.5 Self-folding origamis enabled by uniform heating is a good material for variable stiffness implantation [10].

1.1.3 Variable compliance in medical devices

Surgical operations are highly dependent the ability to maneuver instruments within the human body while causing minimum disruption to healthy organs and tissue. This requirement has motivated building variable body compliance for endoscopy or colonoscopy devices that can dexterously proceed through the complex and fragile environments. Since the path of human intestines are intricately distributed with complex shapes, local body stiffness should be varied in sequence as it proceeds through the human organs or tissues to make safe reorientations as needed. Apart from endoscopic devices which focus on inside body operations [17][18] (figure 1.6), robotic surgical systems such as, da Vinci, are desired to have variable compliance in robotic arm joints to generate different force whist conveying different tasks such as cutting and suturing.

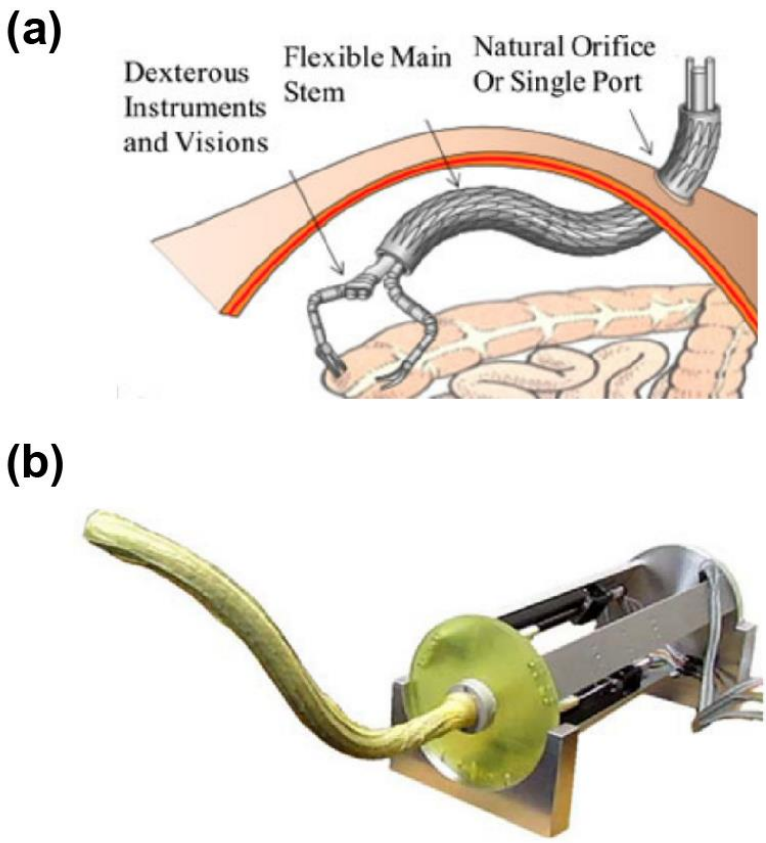

Figure 1.6 A variable stiffness tubular layer design enabling new endoscopes for advanced human body surgery [18] (a) Application of variable stiffness using layer jamming mechanism: flexible main stem used for MIS (minimally invasive surgery). (b) A prototype snake-like manipulator, including three linear actuators based on layer jamming.

1.2 Current approaches in achieving variable compliance mechanisms

To modulate the compliance of a system, many different mechanisms can be applied. Methods such as variable stiffness spring mechanisms, jamming frictions, and nonlinear characteristic of materials under certain excitations, such as shape memory alloys (SMAs), piezoelectricity, magnetorheology (magnetorheological fluids or MR fluids) and electroactive polymers.

1.2.1 Compliance modulations using spring mechanisms

Traditional variable compliant system has been focusing innovative spring designs to achieve variable stiffness actuators (VSAs) or variable impedance actuators (VIAs) [19]. combination and reconfiguration of springs has a large impact of the output force/torque with different motor displacement, meaning the transmission driven by the motor using spring mechanisms can have different compliance as well. For instance, in [20], R. Schiavi et al. have reported a novel prototype of VSA exploiting 2 antagonistic 4-bar transmission mechanisms in opposition. A diagram of 4-bar spring mechanism is shown in figure 1.6, and the compliance seen in point O can be determined by the spring factor as well as the rotary angle theta. Therefore, by adding another 4-bar spring system in an antagonistic way, a joint being connected will then present a variable torque-displacement curvature and thus be used in compliant and safe interactions between human and robots. By using linear control algorithms, the stiffness change can be augmented; however, such a design is highly depended on accurate manufacturing and primarily for mechanical joints, which is limited in other robotic applications.

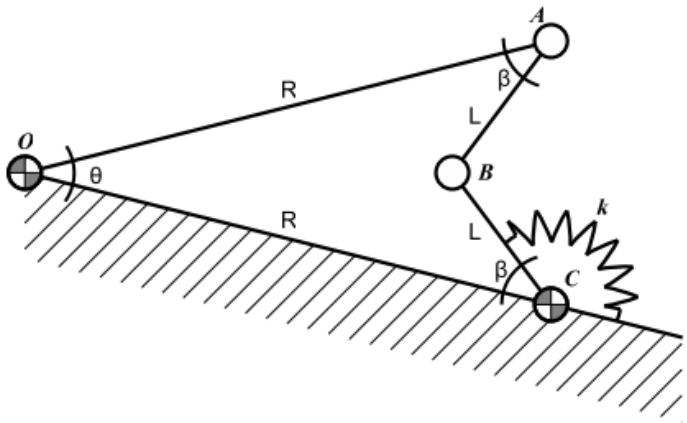

Figure 1.7 Line diagram of 4-bar transmission mechanism of VSA-II [20]. The stiffness seen by point O (driven by a motor) on bar OA is a nonlinear combination of both R, L and k.

1.2.2 Compliance modulations implementing jamming effects

Jamming is the physical process by which the internal friction of some mesoscopic materials, such as granular materials, glasses, or polymers, increases with the increasing particle density [14]. There are 2 main approaches in generating jamming effect by either jamming layers or granular materials. The first one is to exploit the friction present between layers of thin materials and the second one is using the jamming transition of the granular material. The jamming transition from soft state to stiff state is commonly found in granular material, where the relative mobility each granular particle can change the overall rigidity of the material. Therefore, by applying vacuum pump to a mass of granular material for air evacuation, researchers can design new robotics with significant change in compliance. In [13], Eric Brown et al., have provided a universal robotic gripper based on the jamming effect of granular material. In their design, 2 mechanisms are being exploited for secured gripping performance: in the soft state, a mass of granular can flow around the object and conform to its shape. By applying the vacuum, the granular material contracts and hardens quickly to pinch and hold the object without feedback requirement. Such a design is flexible in gripping variable shapes and forms of objects; however, effective jamming transition is usually generated by bulky vacuum pump which can be a problem for portable small scale robotic designs.

1.2.3 Compliance modulations based on material's non-linear characteristics

Apart from using traditional spring mechanisms and jamming effects whose overall rigidity can be tuned using material or structure reconfiguration, materials having non-linear physical properties under changing excitations can be easily adapted for multiple operating requirements. For instance, shape memory alloy can be deformed and return to its pre-deformed under heat [15][22]. During this process, its stiffness varies from low to high and can be incorporated as a

variable stiffness actuator. In [23], A. Hadi et al. used a variable structure control and realized a one-degree-of-freedom actuator based on SMA springs. In [24], C. Majidi and R. J. Wood have designed a tunable stiffness sheet with micro-confined magnetorheological domains at low magnetic field. By combing both SMA and PLA (Polylactic acid) materials, researchers in [25] have present a hybrid design of an active variable stiffness fabric, driven by heat control of SMA and the glass transition temperature, the fabric will conform to different shapes under the same loads; likewise, using non-linearities of materials in designing variable stiffness or compliance structures can also be found in dielectric materials, such as dielectric actuators and elastomers. Based on electrostatic effects (electrostatic chucking) [26], a multi-layered dielectric actuator can display a range of different tip displacement and blocking force under different apply voltages, as shown in figure 1.8. In the meanwhile, in [27], Atsuo Orita et al., have reported a scalable DEP (dielectric electroactive polymer) for variable stiffness suspensions under changing applied voltages. Others been using DEP also achieved certain success on variable stiffness performances [28-32]. However, challenges still exist for the use of DEP as a new generation for variable stiffness devices based on the high voltage requirements, hysteresis and low reliability as compared to other mechanisms.

Though being reversible and effective, all variable compliance mechanisms based on the non-linear properties depended on the external sources usually lack the mobility and is too time consuming to be imported in mobile robots for real time control of stiffness and compliance.

In this sense, current mechanisms in realizing variable compliance are all limited either by high-level input energy requirements or complex spring structures which brings up more challenges in designing and manufacturing. Therefore, new methods in realizing variable compliance

modulation in future robotics are desired as an integrated building block, capable of tuning the material properties in a real-time pattern with little dependence on the external energy sources.

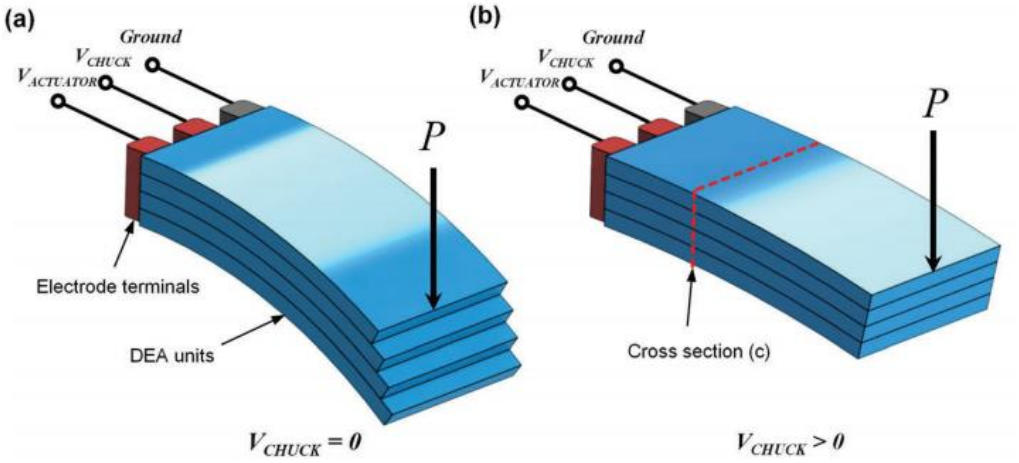

Figure 1.8 Schematic diagrams of VSDEA (variable stiffness dielectric electroactive actuator) [26]. (a) Chucking voltage off (soft state). (b) Chucking voltage on (stiff state).

1.3 Lamination process and laser cutting technologies in achieving new robotic materials

Laminating is the process through which two or more layered substrates are joined together using a bonding agent. The constituent substrates can be composed of films, papers, or aluminum foils. A laminated (or combined) fabric consists of two or more layers, using fabrics, plastics, woods, or metals, bonded closely together by means of an added adhesive, or by the adhesive properties of one or more of the component layers [33]. As for layer-bonding, adhesives are generally applied to the less absorbent substrate, after which the second substrate is pressed against it to produce a duplex, or two-layer, laminate. Such a manufacturing process can help strengthening materials both globally and locally and if designed as a permutation of a matrix embracing fibers positioned in curvilinear paths, a variable stiffness design can be formed with variable stiffness topology. Therefore, traditional materials such as metals, plastics and fabrics

with fixed flexural stiffness can be recombined to display variable compliance using innovative sheet lamination process.

1.3.1 Benefits of lamination process in achieving variable compliance structure

Lamination process has several advantages in robotic designs and fabrications. Using low-cost, common laminate materials such as composite epoxy laminates, polyimide films and papers, soft materials can be combined to have an increased stiffened flexural strength based on the Euler-Bernoulli Beam Theory. The bonding process of the sheets are easily accessed and secured by using different adhesive layers for either thermal or pressure resistance. Such a technology can be further broadened into a with a range of scales for different applications, such as furniture, packages and robotics [34-36]. On the other hand, compared with other variable compliance mechanisms in which either complicated spring mechanisms or non-linear material modulation methods based on high-level energy inputs, materials under lamination process are capable of real-time compliance modulation by inner reconfigurations of the layers and can be easily incorporated into current robotic designs. The control of compliance is then synchronized with the actuation methods which can be boosted for fast real-time compliance modulation depending on the speed of the sliding motion.

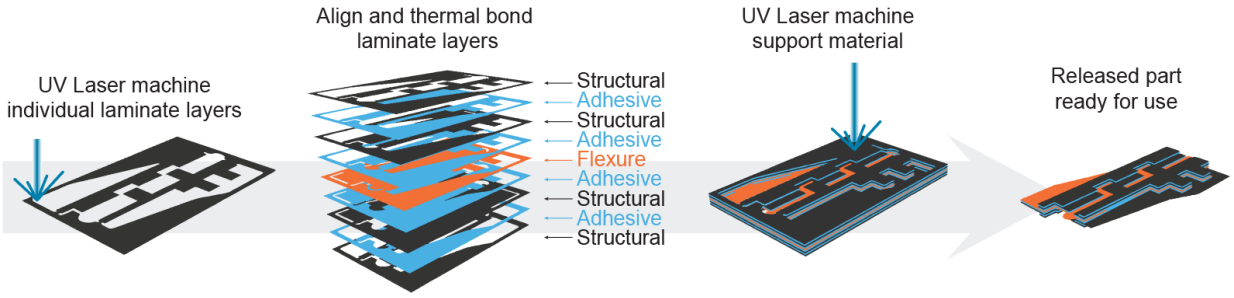

Figure 1.9 Diagrams of lamination procedures in micro air vehicle's hinge fabrication.

1.3.2 Laser cutting technology in achieving versatile design features

Laser cutting technology offers great accuracy and repeatability to achieve versatile geometrical patterns with of each composing layers of the laminated material. Compared with traditional manufacturing such as machining and current additive manufacturing techniques such as 3D printing and soft matter casting, laser cutting technology has a higher accuracy and fabrication speed for both micro and macro scale prototyping. Figure 1.9 illustrates the procedures in both laser cutting and lamination process to achieve micro-scale robotic devices.

Basically speaking, two different fabrication methods can be used to achieve both 2D and 3D design features. The first one is vector cutting, aiming at cutting an 2D outline and a shape of a piece of material. In this action, the laser head starts from a predetermined point and continues along the course of the line until the shape has been cut out. Using this feature, one can realign the laser head onto the project for further cuts. The second one is raster engraving, involving the laser performing a printer-like function as it moves across the material. This action gives 3D features subtracted from the base material, achieved by the material surface being heated by the laser and either fragmenting and detaching from the rest of the surface or by vaporizing the material at that spot on the material. Different depth of features can be tuned by the laser focal point. The result is an engraving that captures the high level of detail present in the raster image design.

1.3.3 Current technology in achieving foldable laminates using lamination process and laser cutting techniques

Researchers using laser cutting technologies and laminating processes have gained great success in developing self-folding structures [19] [20]. These materials are made of either paper or polymer films and have pre-cut patterns with embedded SMAs or SMPs (shape-memory-

polymers) [22]. Under certain actuation methods such as light absorption, resistive heating elements, or environmental uniform heat control. The structure can fold to pre-programmed shapes without human interactions. Compared with traditional manufacturing techniques in which complex 3-D fabrication systems and complicated infrastructures are required for the assembly of these systems, such a bio-inspired folding structure enabled by laser cutting and lamination process is more efficient to meet with little or no infrastructure conditions. In this paper we used laser cutting technology for lamination process and pattern designs, which brings great robustness over a range of different materials, such as FR-4, Kapton, Mylar, and steel sheets.

1.4 Summary

Variable compliance in essential in achieving multi-functionalities of future robotics. In this paper; we present a low-profile, easily fabricated, sheet laminated material capable of modulating compliance as robotic appendage or building blocks for future multi-functional robots. Using thin polyimide films and composite structural sheets such as FR-4, we demonstrated the feasibility of manufacturing a variable compliance layered laminate with pre-defined patterns exploiting both laser cutting technologies and lamination process. By combing and reconfiguring compliant and rigid regions of the layered laminate, a variable compliance mechanism of the whole beam can be achieved repeatedly. The reconfiguration can be generated by either linear sliding motion, named as Sliding Layered Laminate, or individual actuation of structural elements aimed for programmable soft matter and materials. Quite different from traditional compliance changing methods with limitations in either high-level activation conditions or time-consuming control strategies, the SLL prototype is capable of real-time compliance modulation enabled by simple sliding motion and wide range of stiffness with both soft-rigid (binary) states and intermediate stiffness (graded) states available. Such a multi-functional feature can be also implemented into

other physical properties such as viscosity and deformability under the same SLL design concepts. Finally, by choosing different design principles and manufacturing approaches, the SLL can be tailored to suit for different engineering problems, such as micro-robotic actuators, mobile robots' appendages (wings and tails) and medical devices. This work is a foundational step towards the creation of reconfigurable and programmable material with respect to smart structures and materials for future robotics.

The following sections will focus on the conceptual designs and modelling of SLL, the results of different design principles and the demonstrations of different SLL deigns for different applications.

Chapter 2.

Conceptual Designs and Modelling of SLLs

In this section, we present the conceptual design of Sliding Layered Laminates (SLLs), as well as the modelling approach for analytical estimation of the effective variable spring stiffness. A SLL is a multi-stiffness layered laminate composed by soft and rigid segments arranged in a periodical pattern. Such a combined geometrical structure forms a hybrid structure, whose stiffness can be varied by changing aligning states between the soft and rigid regions. As an introduction of the stiffness changing mechanism, we first introduce the concept of aligned and anti-aligned spring stiffness, which is the motivation for making multi-stiffness SLLs. Later, we introduced the conceptual designs of SLLs, including the material composition, design terminologies and the stiffness changing mechanisms. Based on the laminated structure and arrangement, we model the SLL using Rigidity Matrix, composed by the flexural rigidity of each composing segment. We further extend the Rigidity Matrix into a broader stiffness concept, named as EI (E-Young's Modulus, I-2nd moment of area and EI-flexural rigidity). Finally, we provided the theoretical simulations of a long SLL's (composed by 100 SLL units) effective spring stiffness against changing alignments. The result shows great variabilities of SLL stiffness-alignment curvature

under different design principles, which can be further exploited for different applications and fields

2.1 Introducing the dual-stiffness concept

Dual stiffness can be achieved by rearranging the soft and rigid regions within a double layered laminate [2][37]. In figure 2.1, a double-layered laminate consisting of both soft and rigid segments are presented in two different configurations (aligned and anti-aligned). Here we used spring concept to analogize the stiffness regions built in the laminates. With respect to the alignment state of the double-layered laminate, the spring can be arranged in both aligned and anti-aligned states. In this diagram, two pair of springs represent one repeatable stiffness regions (including both soft and rigid regions), with a higher elastic spring factor k_1 representing the rigid region and a lower elastic spring factor k_2 for the soft segment. By calculating the integrated elastic spring factors for both cases, we can always find that the overall spring factor of the anti-aligned spring system is always higher than the aligned spring system. Assuming no friction and jamming effects between the layers, the bending stiffness of the laminate can be taken as elastic spring factors in the direction of the bending moment, and thus be applied as a dual-stiffness structure for multi-functional material designs. The dual-stiffness model can be extended into multi-layered laminate and have multi-stiffness states in aligned states.

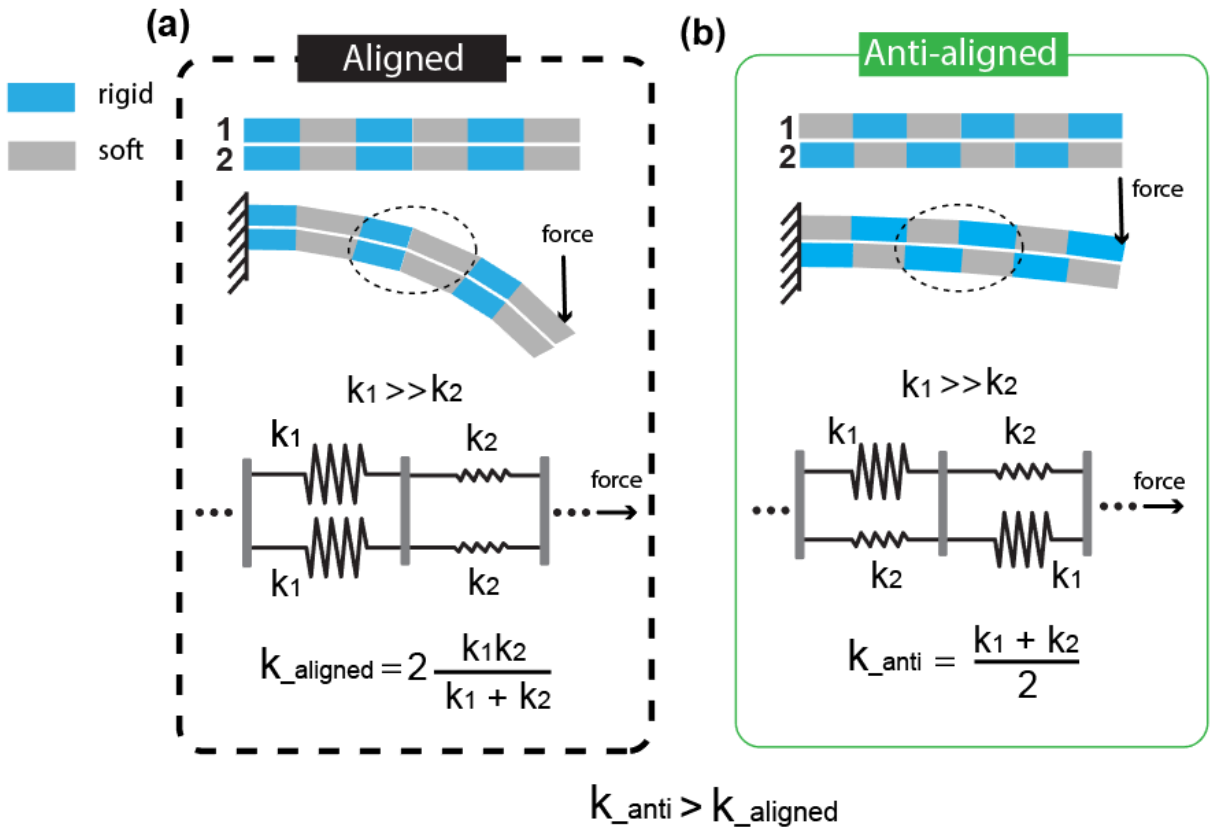

Figure 2.1 Dual-stiffness concept under both aligned and anti-aligned configurations. The combined elastic spring factor is always higher in the anti-aligned state than the aligned state. (a) The aligned state of a double layered laminate and its spring configuration (in parallel). (b) The anti-aligned state of a double layered laminate and its spring configuration (in antagonistic).

2.2 Conceptual design of SLLs (terminology)

Motivated by the dual-stiffness and multi-stiffness structure, we come up with the variable stiffness Sliding Layered Laminate concept based on the changeable configurations of multiple layers composed by both soft and stiff regions arranged in a repeatable pattern. In this section, we define the terminology for SLL's conceptual design to help with the characterization the changing stiffness mechanism in the future sections.

A Sliding Layered Laminate (SLL) is a variable compliance structure with its stiffness changing mechanism based on the sliding motion of its composing laminated layers. A SLL has

multiple laminated layers within its own structure (figure 2.2a). Each laminated layer is composed by soft and rigid regions arranged in a periodically repeatable pattern, with l_{unit} the total length of one laminate cycle of both the soft and stiff regions (l_{soft} and l_{rigid}) (figure 2.2b). The soft region is usually composed by a single-layered material with low Young's Modulus such as, Kapton tape, Mylar and soft fabric; while the rigid regions are generally composed by rigid materials (figure 2.2c), such as FR-4 or metals and has a higher Young's Modulus than the soft region. Based on the periodically segmented patterns each laminated layer has, we can then reconfigure them into different aligning states to achieve a combined variable bending performance based on the sliding motion of the central layer (figure 2.2d). To simplify the laminate reconfiguring mechanism, we constrain the motions of both top and bottom laminates (outer laminates) and only change the relative positions of the central laminate regarding to the outer laminates. In this sense, the laminate's aligning state is solely depended on the central laminated layer and can be reversed and repeated to achieve a periodic stiffness variation of the whole laminate. The SLL's bending performances can be then divided into stiff, intermediate and soft state corresponding to the aligning configurations and be reversibly tuned based on the sliding motion of the central layer (figure 2.2e). Since the stiffness regions are arranged in a periodical pattern along the lengthwise-direction of the laminate, we then focus on the theoretical modelling of one repeatable SLL unit of the infinitely long laminate and use the aligning percentage (figure 2.2d) as the main parameter to characterize the variable stiffness under changing alignment states (figure 2.2f). The bending performance of one SLL unit can be propagated to the whole laminate using Euler Bernoulli Beam Theory and will be further discussed in the next section.

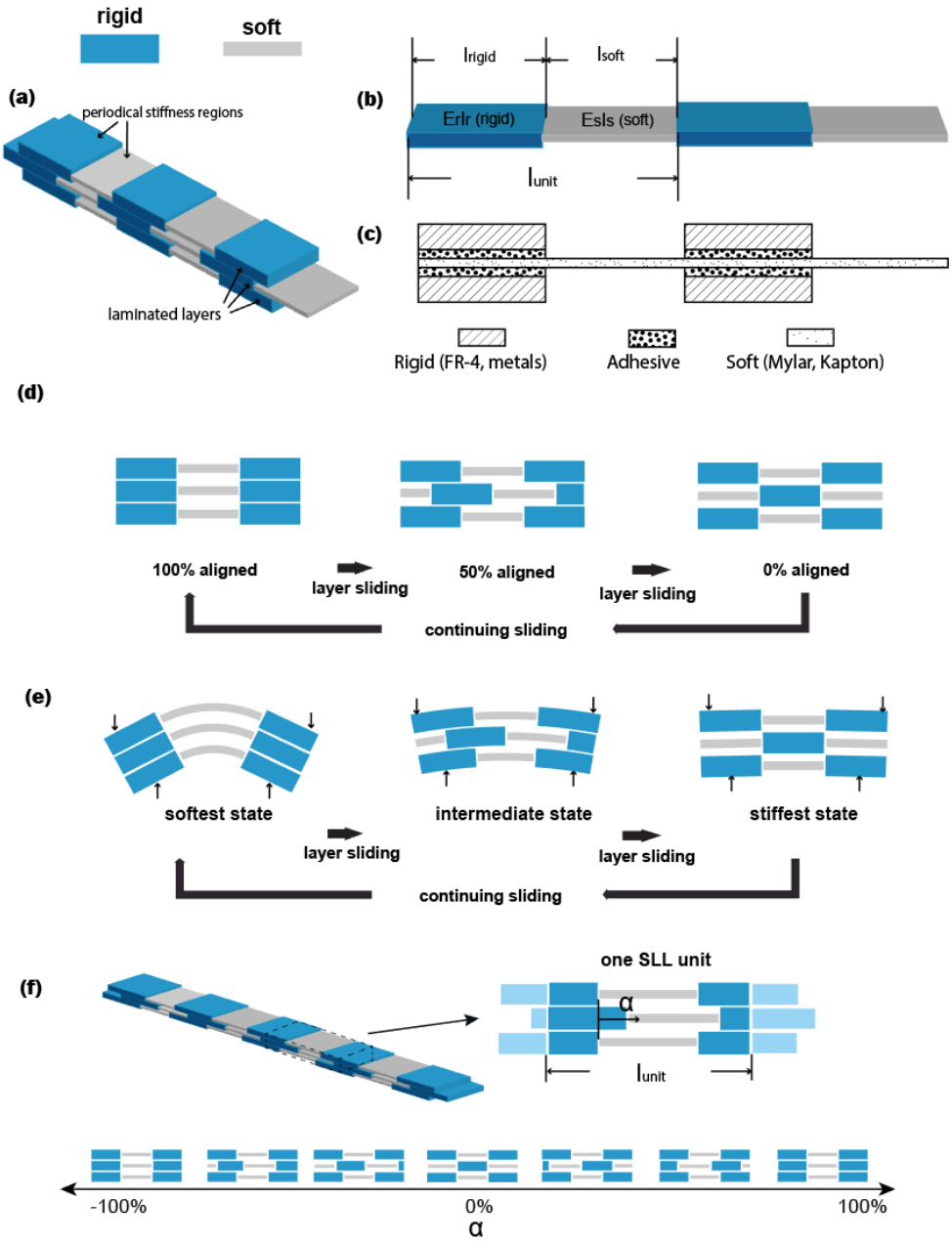

Figure 2.2 Conceptual designs of SLLs (a) Isometric view of a SLL composed by multiple layered laminates with periodic stiffness regions. (b) Length parameters for one laminated layer and one SLL unit. (c) Schematic cross-section of the material composition for one laminated layer. (d) A sliding-layer mechanism for stiffness modulation of the whole SLL based on the reversible sliding motion of only the central laminated layer. (e) Effective spring stiffness changed by the sliding motion of the central layered laminate with respect to the aligning states in (d). (f) The demonstration of one SLL unit as a modelling module, which can be propagated to the whole SLL for stiffness prediction. The aligning percentage, α is defined as the layer approaches the stiffest state from the softest state varying from (-100% to 100%).

2.3 Modelling of SLLs

The conceptual design and modelling are based on a long SLL (including 100 beam units) composed by three laminated layers. Since a beam unit can be shortened or elongated to meet different scales of applications, a long SLL will reveal smooth bending stiffness variation under the sliding motion of the central laminated layer. In the modelling, we assume no friction or jamming effects between each laminated layer and the bending curvature is caused by pure bending moment which are predicted using the Euler Bernoulli beam theory. We first characterize the structural feature of the SLL, the flexural rigidity, as a Rigidity Matrix to simplify the geometrical feature of each SLL unit. We then integrate the Rigidity Matrix into a 1D load carrier and use Euler Bernoulli beam theory to further predict the SLL bending stiffness based on one end fixed cantilever beam test. Such a prediction method, although based on a long SLL, can be scaled to suit for a constrained SLL design. The variation of different stiffness changing curvatures are manipulated based on three main design parameters and will be further discussed in the following sections. Our goal is to vary the stiffness changing feature under the sliding motion (the aligning percentage α) with different design parameters to guide multi-purpose SLL fabrications.

2.3.1 Flexural rigidity and Euler-Bernoulli beam theory

Flexural rigidity (defined as EI), is the force couple required to bend a non-rigid structure in one unit of curvature [22]. A beam or rod with varying flexural rigidity (EI) is expressed as

$$EI\frac{d\omega}{dx} = \int_0^x M(x)dx + C_1 \tag{2.1}$$

where E is the Young's modulus (in Pa); I is the second moment of area (in m^4); ω is the transverse displacement of the beam at x, and M(x) is the bending moment at x; C_1 is the integral constant due to the boundary conditions of the bending motion. Flexural rigidity is also defined as the

resistance from a structure undergoing certain bending force or moment. In the study of geology, the flexural rigidity of a thick plate is determined by the Young's modulus, Poisson's ratio and cube of the plate's elastic thickness, and can be expressed as

$$D = \frac{Eh_e^3}{12(1-\nu^2)} \tag{2.2}$$

where E is the Young's Modulus (Pa), ν is the Possison's Ratio and h_e is the elastic thickness (m). Flexural rigidity is the bridge between the beam deflection of each point and the external loads the structure undergoes which can be used to further calculate the bending stiffness at a certain point under certain constraining methods. In this paper, the flexural rigidity is the main parameter used to characterize different stiffness regions of the SLL, with E_rI_r the flexural rigidity of the rigid regions and E_sI_s of the soft regions.

Euler Bernoulli beam theory is a simplification of the linear theory of elasticity which provides a means of calculating the load-carrying and deflection characteristics of beams. The Euler-Bernoulli equation describes the relationship between the beam's deflection and the applied loads, which can be expressed as

$$\frac{d^2}{dx^2}(EI\frac{d^2\omega}{dx^2}) = q \tag{2.3}$$

where q is the distributed load (force per unit length), and can be a function of x, ω. Generally, we use M(x), as the load source and rewrite (2.3) as

$$M(x) = EI(x)\frac{d^2\omega(x)}{dx^2} = EI(x)\kappa \tag{2.4}$$

where EI(x) is the flexural rigidity of the structure at a certain point and κ is the curvature of the bending curve. The deflection at each point can then be integrated for the laminate displacement and be used to calculate the bending stiffness at a certain point under certain load conditions. In

this paper, we use fixed end cantilever testing method and a concentrated load at the free end to estimate the tip displacement and further calculate the bending stiffness of the structure as shown in figure 2.3.

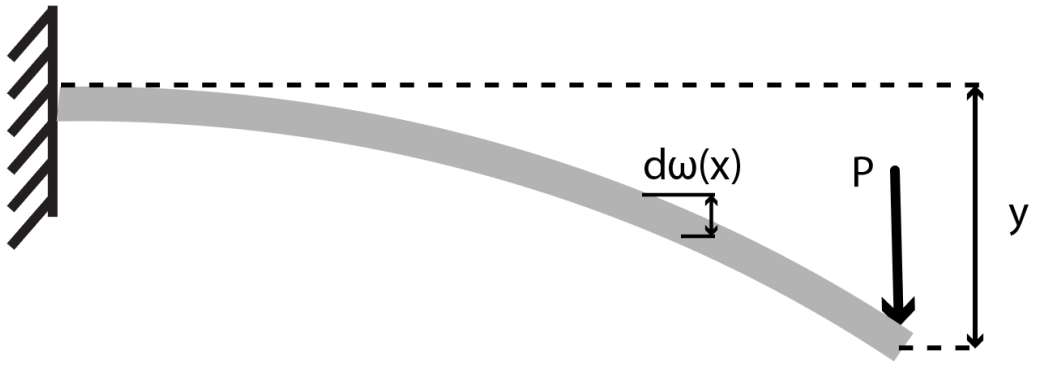

Figure 2.3 A cantilever beam test for calculating the bending stiffness of an elastic beam structure.

2.3.2 Bending stiffness of an elastic beam

The bending stiffness of an elastic beam is focused on the tip displacement under external point load condition (figure 2.3). It is defined as

$$K = \frac{P}{y} \tag{2.5}$$

where K is the effective spring stiffness of the SLL (in N/m), P is the point load applied at the free end (in N), and y is the tip displacement (deflection) in the vertical direction.

To solve for the bending stiffness, we integrate the deflection ω(x) at every consecutive point of the SLL and rewrite y as

$$y = \int_{L_t} d\,\omega(x) \tag{2.6}$$

where Lt is the total interval of the beam undergoing the load condition. From (2.4) we know that, the beam deflection ω(x) is related with the bending moment M(x) and the flexural rigidity E(x)I(x) at each consecutive point and could be rewritten as

$$\frac{M(x)}{E(x)I(x)} = \frac{d}{dx}\left(\frac{d\omega(x)}{dx}\right) \tag{2.7}$$

which means

$$\frac{d\omega(x)}{dx} = \int_{L_t} \frac{M(x)}{E(x)I(x)} dx \tag{2.8}$$

By replacing (2.6) with (2.8), we have

$$y = \iint_{L_t} \frac{M(x)}{E(x)I(x)} dxdx \tag{2.9}$$

Thus, the bending stiffness can be expressed as

$$K = \frac{P}{y} = \frac{P}{\iint_{L_t} \frac{M(x)}{E(x)I(x)} dxdx} \tag{2.10}$$

In the cantilever beam test, we can replace the external load condition as

$$M(x) = P(L - x)$$

The bending stiffness can be finally written as

$$K = \frac{P}{\int\int_{L_t} \frac{P(L-x)}{E(x)I(x)} dxdx} = \frac{1}{\int\int_{L_t} \frac{(L-x)}{E(x)I(x)} dxdx} \tag{3.3}$$

From the final equation of the bending stiffness we find that, the bending stiffness of the SLL is independent of the external load conditions and can be varied by the variable flexural rigidities along the lengthwise direction of the beam structure as well as the total length of the beam. The derivations of the bending stiffness for a beam structure serve as the theoretical

foundation of variable stiffness SLL and proves the idea of changing aligning state for bending stiffness modulation.

2.3.3 Rigidity Matrix and EI profile of SLLs

The stiffness of a composite laminate can be processed different based on the geometrical feature it possesses. In [24], three different approaches have been reported and compared to estimate laminate stiffness using stiffness matrices, which requires complex mathematical apparatus. In [25], the stiffness was considered as the pure sum of the flexural rigidity of each composing layer which lacked the generality in considering other design parameters such as length and beam patterns. Still both are applying the strategy in combining the structural elements from individual beam component to construct the overall stiffness of the composite laminate. In this paper, the concept of Rigidity Matrix and EI profile have been reported for the first time. By integrating the flexural rigidity from each laminated layer into a 1-D load carrier (an elastic beam model), we predict the variable stiffness of each aligning state from the softest to the stiffest state of the SLL. Again, we assume no frictional or jamming effects between layers and the strains of each layer are caused by pure bending moments.

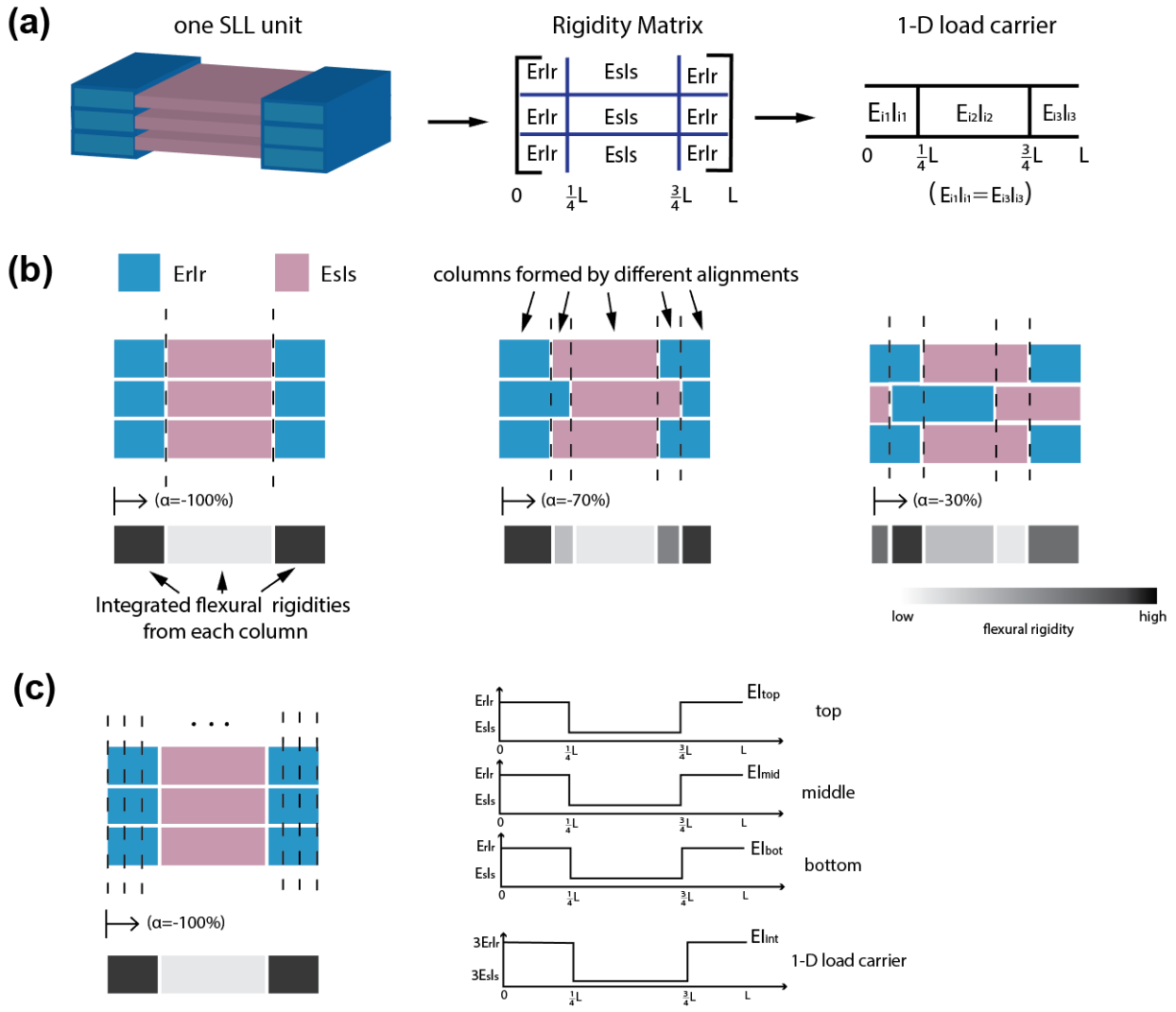

Figure 2.4 Diagrams of the Rigidity Matrix concept and the conversion of the flexural rigidity form the Rigidity Matrix to a 1-D load carrier. (a) The Rigidity Matrix and its EI values listed in the same configuration. The 1-D load carrier has the integrated flexural rigidity in corresponds to the Rigidity Matrix alignment state. (b) The Integrated EI values of different aligning percentage. The grey bar shows the difference of the stiffness topology between each alignment state. (c) The SLL unit characterized using EI functions, with flexural rigidities EIs along the longitudinal direction.

Specifically, each soft/rigid region of one SLL unit can be modified as a structural element with 2 characterizing parameters, the flexural rigidity EI and the geometrical length l. For different aligning states of the SLL, we then list all the flexural rigidity values for each segmented element in the same laminate configuration (figure 2.4a). For different aligning states of one SLL unit, we then combine the flexural rigidity from multiple laminated layers column-wisely to form a 1D load

carrier. The 1D load carrier will then have variable flexural rigidity along its length direction which could be plugged into (3.3) for the bending stiffness calculations.

The integration of EIs is based on the moment curvature relationship and derived as follows: Suppose we have multiple (n) sub-laminates within one column of the Rigidity Matrix with homogeneous flexural rigidity E_iI_i (i=1, 2, 3…, n) of each element from the top to the bottom layer (figure 2.5). The parameters for the composite elastic beam is listed below,

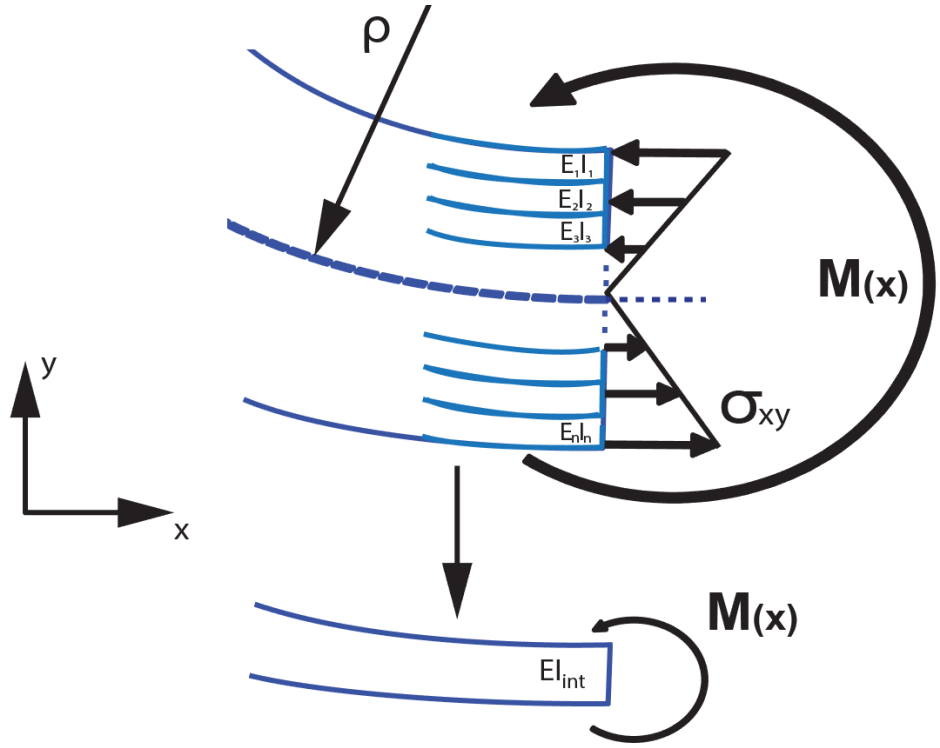

Figure 2.5 Diagram showing the integration of the flexural rigidity from each composite beam element into one beam unit

A, cross-sectional area of the whole beam,

A_i, cross-sectional area of each beam component,

M(x), the bending moment,

σ_{xy}, the stress on the cross-sectional surface,

y_i, the distance of each layer to the neutral axis.

$$M(x) = -\int_A \sigma_x y dA = -\sum_{i=1}^{n} \int_{A_i} \sigma_x y_i dA_i \tag{2.11}$$

Given the neural axis, we have

$$\sigma_x = E_i \varepsilon_x = -E_i \frac{y_i}{\rho} = -E_i y_i \kappa \tag{2.12}$$

where ρ is the radius of the curvature shaped by the bending moment M(x), inserting (3.5) into (3.4) we have

$$M(x) = \kappa \left(\sum_{i=1}^{n} E_i \int_{A_i} y_i^2 dA_i\right) \tag{2.13}$$

Recalling the 2nd moment of area of each sub-laminate with respect to the neural axis.

$$I_i = \int_{A_i} y^2 dA_i \tag{2.14}$$

Thus, by combining (2.13) and (2.14), we get

$$M(x) = \kappa \left(\sum_{i=1}^{n} E_i I_i\right) \tag{2.15}$$

Recalling Euler-Bernoulli beam theory (2.4), we have

$$EI_{int} = \sum_{i=1}^{n} E_i I_i \tag{2.16}$$

where EI_{int} is the integrated flexural rigidity for all the composite beam elements stacked in the same column. This formula means that the flexural rigidities from all bending components can be added along y axis, which serves as the basis for integrating Rigidity Matrix into a 1D load carrier for simplified stiffness calculation.

We then integrate the Rigidity Matrix column-wisely into a 1D load carrier for simplified stiffness estimation (as shown in figure 2.4b). Each alignment state (aligning percentage) corresponds to one specific configuration of the 1-D load carrier and the flexural rigidity

distribution along the load carrier. The changing topology of the flexural rigidity along the load carrier will then display a variable bending stiffness feature under certain load conditions.

Based on the integrated flexural rigidity concept from each element of the Rigidity Matrix, we further characterize the SLL unit as a multi-layered EI profiles which could be summed based on the integrated flexural rigidities from each laminated layer. The EI profile can be taken as a flexural rigidity function of the position in the length-wise direction of the laminate. Based on the previous integration methods of Rigidity Matrix, a SLL unit can be divided into an infinite number of EI columns and summed, meaning that each laminated layer can be characterized as a function with changing EI values and be linearly added. Depending on the geometrical design features of the SLL, the EI profile of each composing laminate may vary either in a sinusoidal wave or a binary pattern. The material composition, the layer thickness and the length of soft/stiff regions will also affect the EI profiles.

2.4 Stiffness simulations based on three design principles

From the perspective of EI profile, different design parameters will have a big influence in manipulating the stiffness-alignment curvature under the sliding motion of the central layer. In this section, we explored three design principles in manipulating the stiffness-alignment curvatures.

2.4.1 Introduction of three main design principles

We summarized three main design principles in SLL fabrication for different bending performances under the laminate sliding motion. 1. The E_rI_r and E_sI_s, are the flexural rigidities of the rigid and soft regions. By changing the material composition of the composite laminate, we can change the stiffest and softest stiffness as well as the intermediate states under the layer sliding motion (figure 2.6(a)). 2. The aspect ratio of SLL unit is defined as the length of the rigid regions

in portion of the whole length of the SLL unit. By choosing different aspect ratio of each laminated layer, the overlapped regions in the stiffest state will vary to achieve either longer or shorter stiffest state (figure 2.6(b)). 3. By changing the design patterns of the SLL of each unit, the curvature will become either graded or binary (stiffness sensitivity) depending on the design patterns of the SLL unit (figure 2.6(c)). From an EI profile perspective, these three design principles can change the profile from three basic perspectives, which are the duty factor of the rigid EI, the limits and amplitudes, and the waveforms of the profiles.

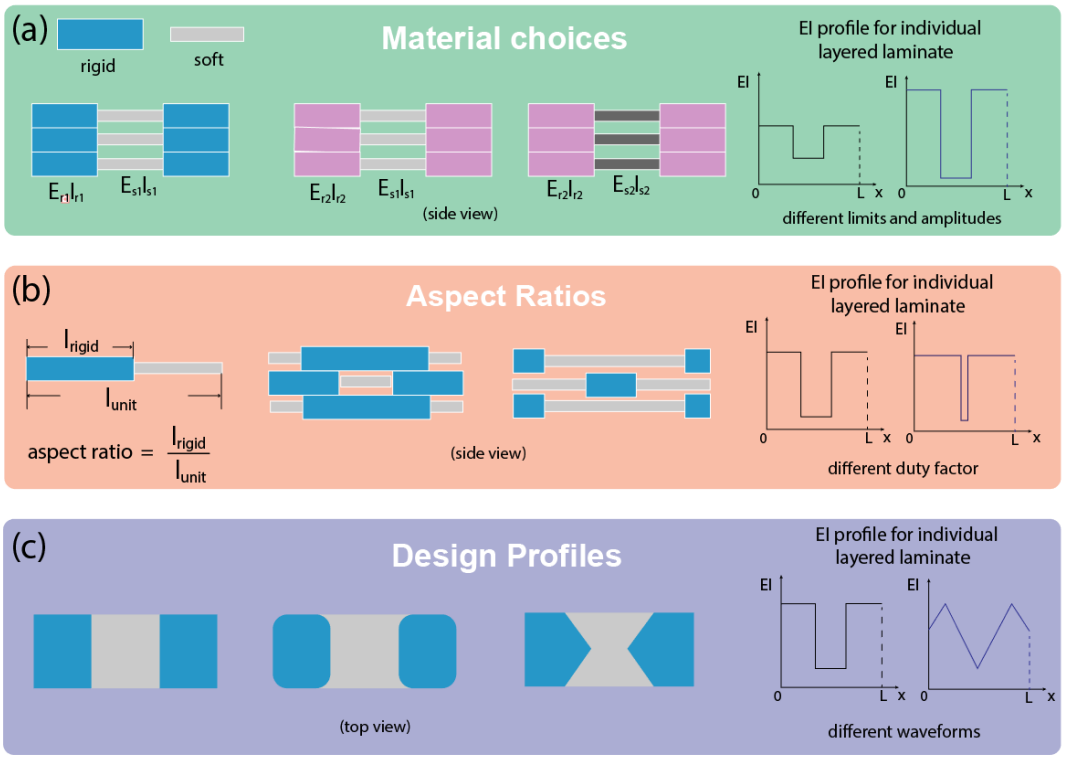

Figure 2.6 Three design principles affecting SLL stiffness modulation from three aspects of the EI profiles. (a) The material choices, defined as changing the flexural rigidities of soft and rigid regions, affects the lower and upper limits of the EI profiles. (b) The aspect ratio, defined as the length of the rigid regions in portion of the whole length of one beam unit, affects the duty factor of the on state in portion of one EI period (beam unit). (c) The design profiles, defined as the longitudinal stiffness patterns from the vertical view, affects the shape of the periodical EI profile within one beam unit.

2.4.2 Changing E_r/E_s for stiffness-alignment curvature modulation

In this part, we demonstrate the influence of changing the flexural rigidity of the composing element from a material composition perspective and discuss the result of a simulated stiffness variation under the sliding motion/ alignment states.

The stiffness simulation is done over a long SLL including 100 beam units. Each beam unit is assigned with unit length (L=1) with no dimensions. The aspect ratio of the SLLs' unit is 50% ($l_{rigid}=l_{soft}=1/2l_{unit}$). The effective spring stiffness is expressed in terms of ErIr or EsIs depending on the controlled variable in each case (constraining ErIr while changing EsIs or constraining EsIs while changing ErIr).

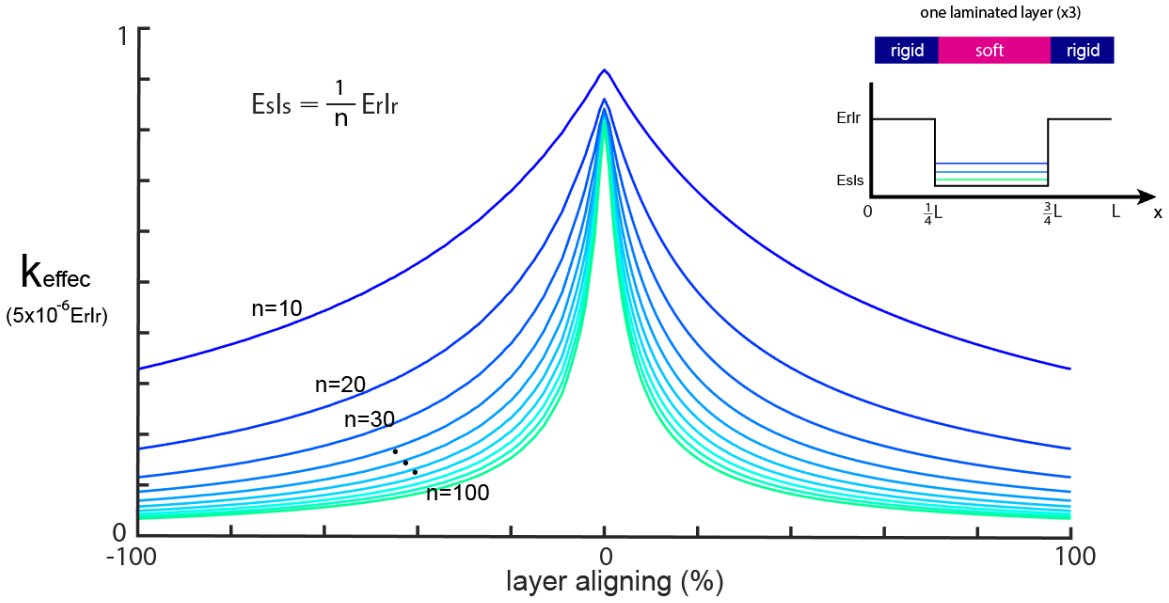

Figure 2.7 the predicted bending stiffness of a SLL with 100 units (unit length=1) under changing EsIs (EsIs=1/n*ErIr) but constant ErIr, where n varies from 10 to 100. The upper right diagram shows the EI profile of each laminated layer (three laminated layers in total). The SLL unit is composed by 3 identical laminated layers with only the central layer under sliding motion for stiffness modulation.

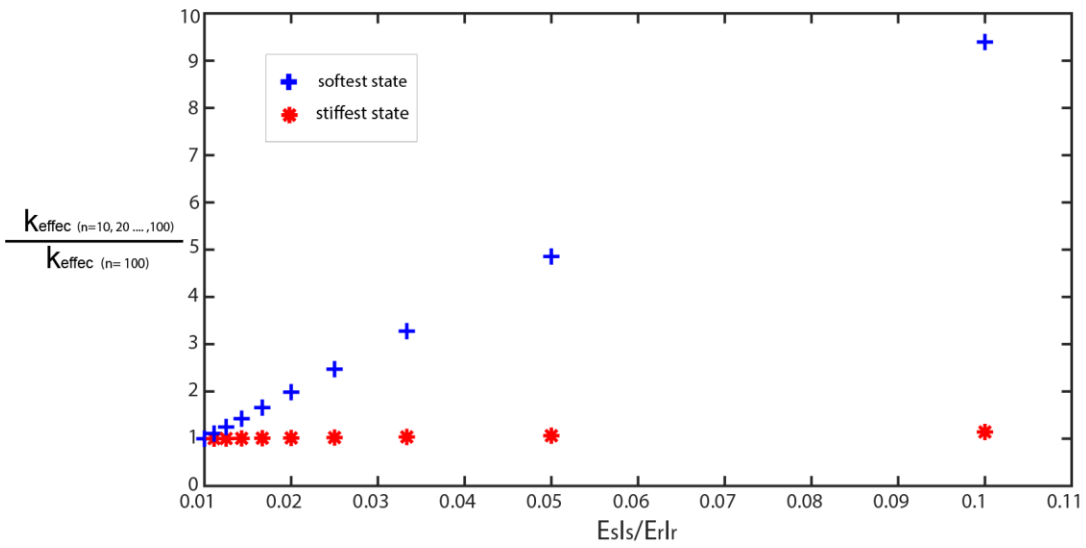

Figure 2.8 The gain of effective spring stiffness only at softest/stiffest states between each EsIs/ErIr case and the one only at n=100.

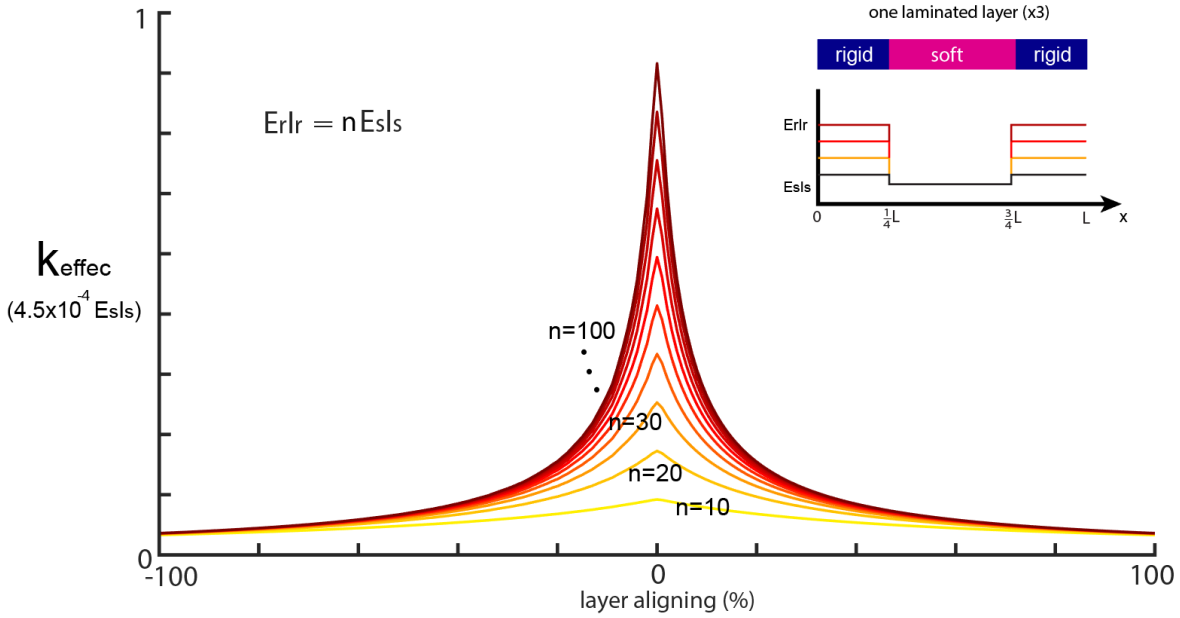

Figure 2.9 the predicted bending stiffness of a SLL with 100 units (unit length=1) under changing ErIr (ErIr=n*EsIs) but constant EsIs, where n varies from 10 to 100. The upper right diagram shows the EI profile of each laminated layer (three laminated layers in total). The SLL unit is composed by 3 identical laminated layers with only the central layer under sliding motion for stiffness modulation.

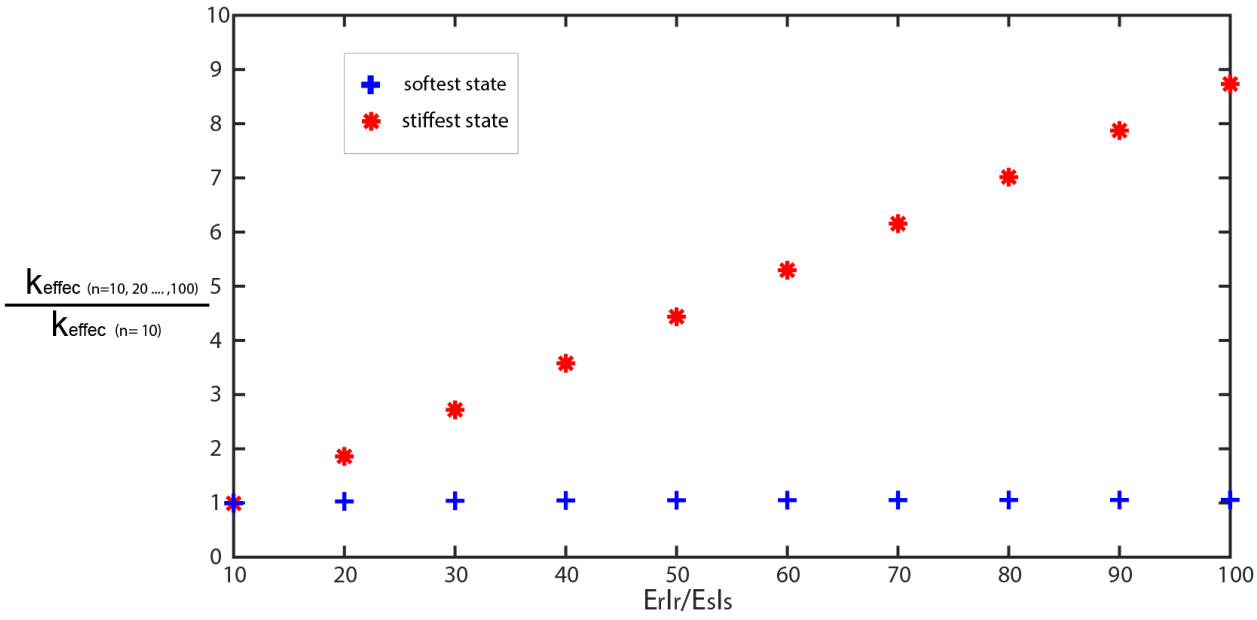

Figure 2.10 The gain of effective spring stiffness only at softest/stiffest states between each ErIr/EsIs case and the one only at n=10.

Figure 2.7 shows that the effective spring stiffness of the stiffest state is largely depended on the flexural rigidity from the rigid regions. By increasing the material EI values of the rigid regions, the keffec at the stiffest state will be linearly increased (figure 2.8). On the other hand, the effective spring stiffness of the softest state is determined by the change of flexural rigidity or material composition in the soft regions (figure 2.9 & figure 2.10). Using this concept, the range of effective spring stiffness of the SLL can be either extended or shortened for different applications. Note that the increasing EsIs also helps with increasing the intermediate stiffness values of the curvature, which enables the SLL to change in a graded pattern, but narrows down the stiffness change range on the other hand. This tells us that changing the flexural rigidity (material composition) of the SLL would effectively change the stiffness varying range and be used for areas where high stiffness gains are needed.

By changing both ErIr and EsIs, and increase them to be a certain fold of a constant flexural rigidity value, for instance, E0I0 (with ErIr=n*E0I0, and EsIs=0.1ErIr), we find the stiffness-

alignment curvature being shifted, as well as the stiffness for both the stiffest state and softest state being raised with the same fold change. Figure 2.11 and 2.12 demonstrate how increasing the flexural rigidity for both regions will affect the stiffness-alignment curvature of the SLL under different alignment states. Thus, changing the flexural rigidity for both soft and rigid regions can then be regarded as a method to shift the overall stiffness property of the SLL but maintain the range of stiffness variation for different applications and areas.

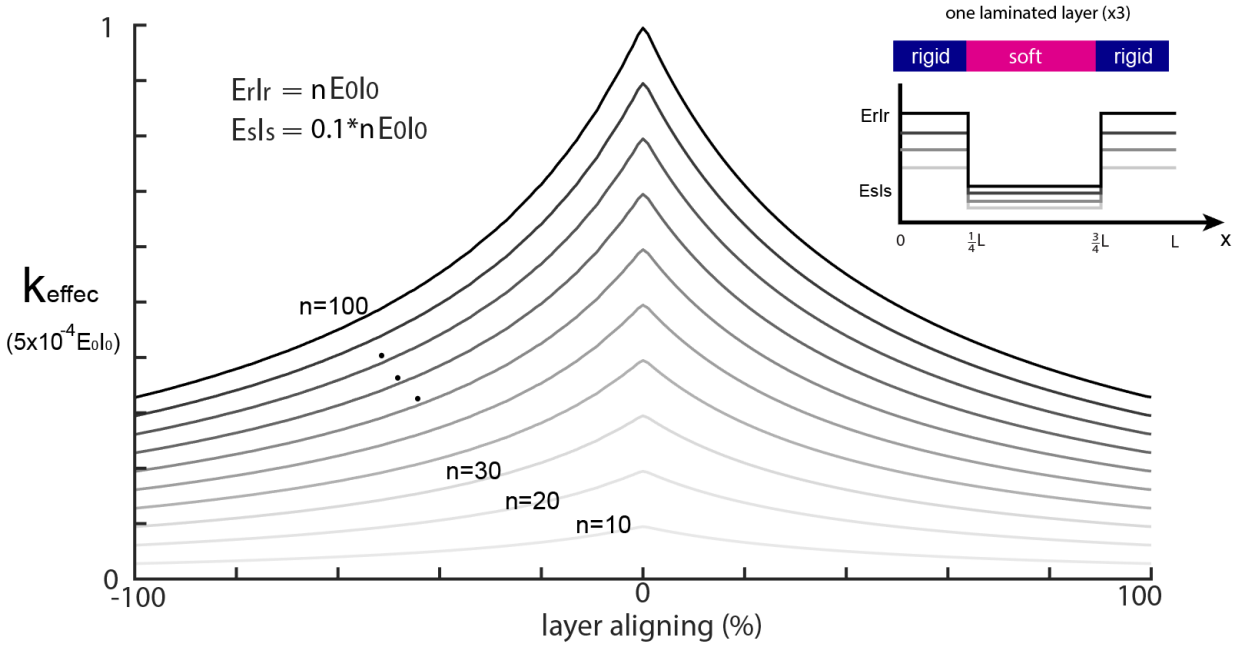

Figure 2.11 The simulated bending stiffness of a SLL with 100 units (unit length=1) under changing ErIr and `EsIs (ErIr=nE0I0, EsIs=0.1n*E0I0, n=10, 20, 30 … 100). The upper right diagram shows the EI profile of each laminated layer (three laminated layers in total). The SLL unit is composed by 3 identical laminated layers with only the central layer under sliding motion for stiffness modulation.

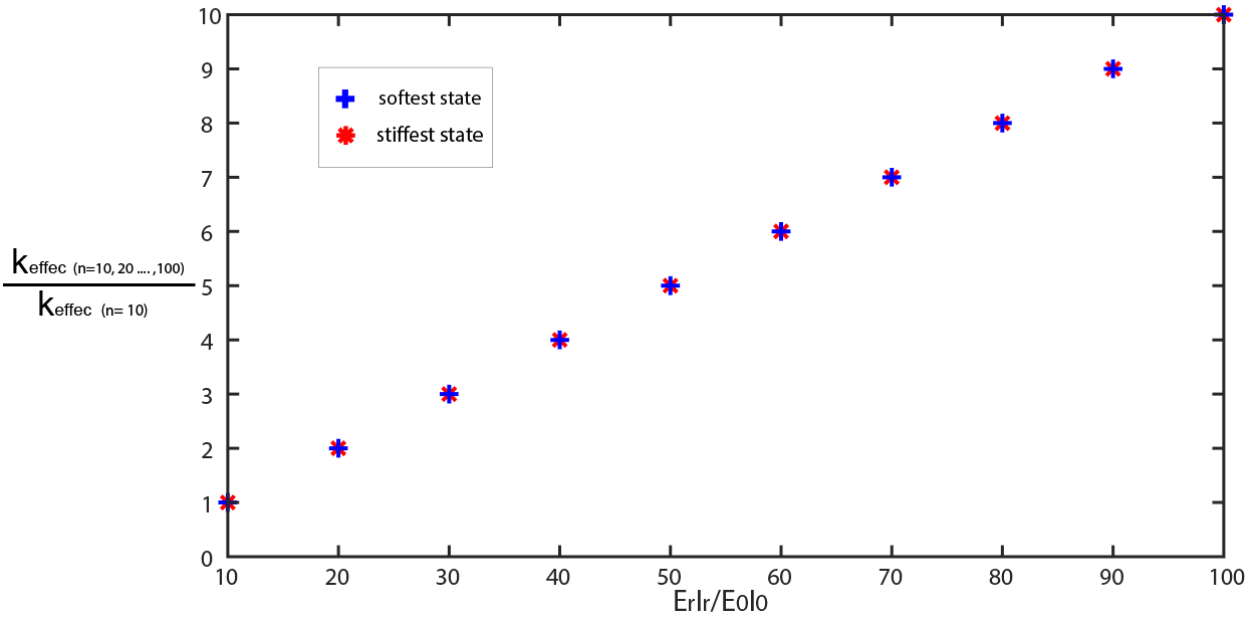

Figure 2.12 The gain of effective spring stiffness only at softest/stiffest states between each ErIr/E0I0 case and the one only at n=10.

2.4.3 Changing SLL's aspect ratio for stiffness-alignment curvature modulation

Changing the SLL's aspect ratio will directly change the overlapping areas of 2 laminated layers in the stiff state, where two rigid regions forms a cage surrounding the soft region and contributes to most of the bending motions (as shown in figure 2.6 (b)), which further affect the stiffness-alignment curvature of the SLL. In this section, we provide 6 scenarios for different aspect ratios of a long SLL (consisting of 100 SLL units, with unit length=1), ranging from 50% - 100%. We also set the ErIr=10EsIs, and the result is expressed in terms of ErIr.

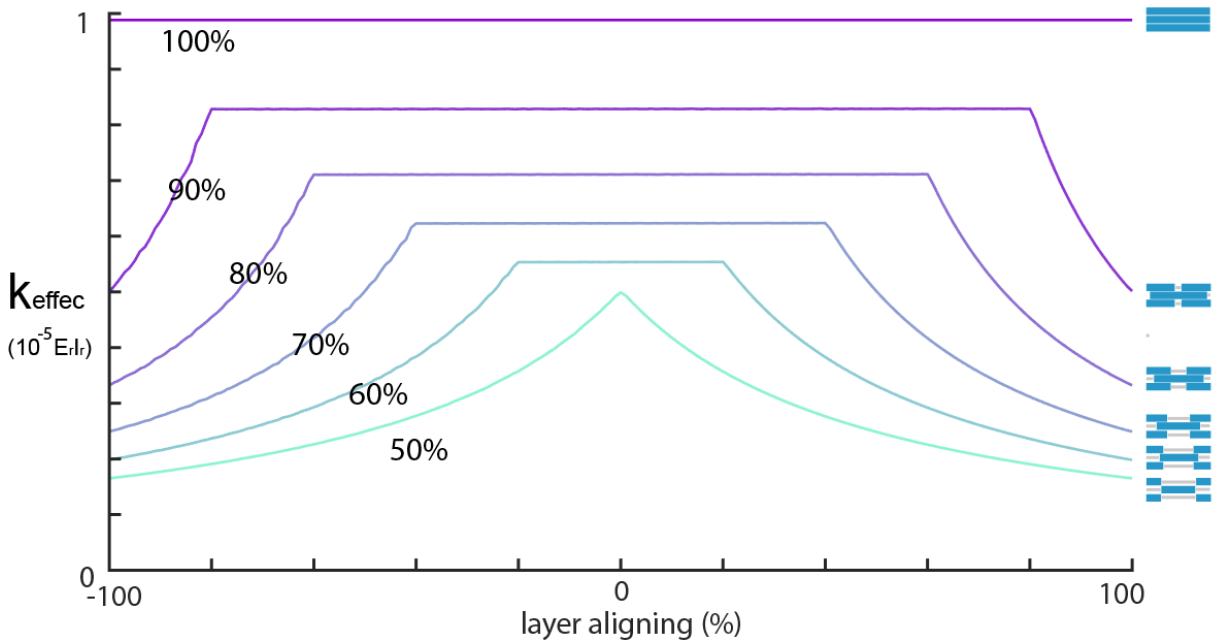

Figure 2.13 Changing aspect ratio of the SLL unit for stiffness-alignment curvature modulations. The right shows the diagram of the corresponding stiffest states with different overlapping areas.

From the plot we can see that, the range of stiffness variation will be less and less as we increase the aspect ratio from 50% to 100%. In the case of 100% aspect ratio, there is no variation of the stiffness-alignment curvature since the sliding motion makes no difference of the alignment states. From aspect ratio 50% to 90%, the stiffness in the both the stiffest state and the softest state are raised. The range of the sliding motion is extended to achieve the stiffest stiffness state. This means that for applications of SLL, the stiffest state becomes easier to achieve with higher aspect ratios, since the sliding motion is always linked with certain actuation source and energy consumption, and the relative sliding distance can be shortened if only a stiff bending performance is needed. On the other hand, for cases of lower aspect ratios, the stiffness-alignment curvature becomes more graded, and the stiffness can be gradually manipulated with multiple intermediate states available. The difference of lower aspect ratio and higher aspect ratio designs mainly lies on the desires for either higher or graded stiffness performance.

2.4.4 Changing SLL's design patterns for stiffness-alignment curvature modulation

Instead of having a binary EI profile of each laminated layer as been mostly discussed in the previous cases, we can also design SLL with other waveforms, such as sinusoidal and triangular wave forms and further discuss the results of stiffness-alignment curvature in these scenarios.

In this section, we first provide an algorithm in calculating waveforms for EI profiles from a sinusoidal wave to a square-like wave using one single parameter. We then list a series of different waveforms generated and calculate the corresponding stiffness-alignment curvatures.

In the waveform generation, we used the sine wave as the starting waveform (with a=1 as the characterizing parameter, which equals to the frequency of the sine wave). We then increase a but only include one cycle of sine wave in the interval of the first case. And use a straight line to connect the peaks and valleys as shown in figure 2.14.

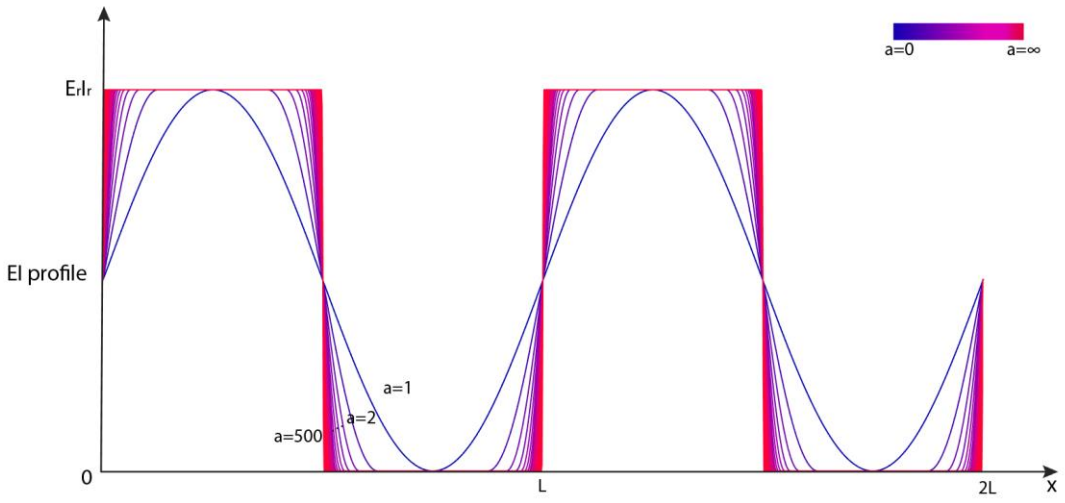

Figure 2.14 The waveform generation of the EI profile for each laminated layer based on one characterization parameter from a=1 to a=10 (from sinusoidal to square waves), with aspect ratio 50%. The SLL is still composed by 100 units, with each unit length L=1.

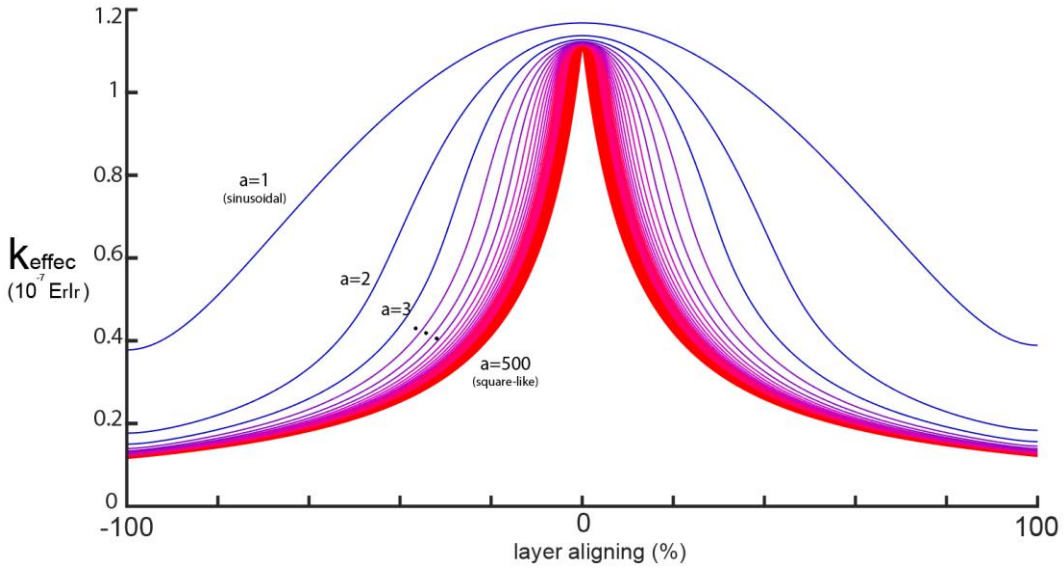

Figure 2.15 Simulated bending stiffness of a SLL with 100 units (unit length=1), aspect ratio 50%, under changing wave forms from a=1 to a=500 (sinusoidal to square-like waves). The SLL unit is composed by 3 identical laminated layers with the same EI profile under variable aligning states.

In figure 2.15, the sinusoidal EI profile helps with increasing the bending stiffness during the sliding motion of the intermediate states, making a more gradual change of bending stiffness from the softest state to the stiffest state. This is because the EI profile has more gradual change from the soft region to the rigid region which makes the average flexural rigidities of the whole layer higher than the binary cases (square-like EI profiles). On the other hand, in the cases of square-like waves, since we are using an aspect ratio of 50% in laminate design. The curvature is spiny in the stiffest state and most part of the sliding motion can only generate a low bending stiffness which can be applied for binary change of bending stiffness. This shows that the distribution or topology of stiffness along one laminated layer can have significant changes in the effective spring stiffness of the SLL under the same sliding motion. For many different applications, we can then build SLL according to different design principles which would result in variably many bending performances.

2.5 Summary

In this chapter, we first present the concept of dual-stiffness structure with the explanatory analogy of spring stiffness under different configurations. We then introduce a multi-layered SLL with multiple bending stiffness and define the terminology for each elemental component. The SLL, based on the sliding motion of the central layer, can display variable stiffness-alignment curvatures under three basic design principles, which correspond to the change of EI profile of each laminated layer from the perspective of duty factor, EI limits and the waveforms. We then simulate the overall bending stiffness of a SLL composed by 100 units based on the different design parameters and demonstrated its great variabilities in the bending performances under continuously shifted alignment states.

Chapter 3.

SLL Fabrication

This chapter focuses on the manufacturing process of the SLL including the design iterations and fabrication tools exploited. SLLs are composed by three laminated layers with both rigid and soft regions arranged in a periodic pattern. Our fabrication approach is based on inexpensive, repeatable lamination process with the help of laser cutting technology. The material choices, design drawings and the fabrication procedures of the SLL are thoroughly discussed in this chapter.

3.1 The material selections of SLL fabrication

The materials selected for SLL fabrication vary over a broad range of materials with different flexural rigidities. Based on previous modelling of SLL under different design principles, the material selections are highly important for either significant change in a dual-stiffness changing pattern or gradually changed stiffness-alignment curvature with multiple intermediate stiffness states. As previously mentioned, the rigid (structural) parts (FR-4, steels, coppers), the compliant films (Mylar, Kapton), the adhesive films (double-sided adhesive films) and the boundary layers (either Scotch tape or the combination of both compliant and adhesive films) are necessary for the fabrication of multi-stiffness SLL structure.

For the rigid parts, we usually choose FR-4 as an elastic high-stiffness bending component. FR-4 is a composite material composed of woven fiberglass cloth with an epoxy resin binder which is flame resistant. Compared with steels and coppers, FR-4 can be easily cut using laser cutting technology (by the Universal laser system from Prof. Tolley's Lab). Also, we used FR-4 from 0.005 to 0.25 inches to change the E_rI_r and E_sI_s for different testing samples (FR-4 can be used as components for SLL's soft regions as a thin strip). In some cases, we used steels and copper sheets for based on their elasticity and ductility and incorporate them as ductile SLL for energy dissipative functions (further discussed in the late sections).

For the soft films, the benefits of using Kapton arrive from 2 sides: one is its softness (low flexural rigidity) generating large bending motions even under a small activation force; the other one is its low surface roughness enabling smooth sliding motions between each laminated layer, if being coated as a sliding surface. Due to its smoothness, Kapton can be easily adhered to rigid sheets (FR-4, or coppers) easily for a long time which makes it a better solution for composing the soft regions. For large-sized SLL fabrication, we also used Mylar as compliant materials for soft regions. Since Mylar is usually thicker and stiffer than Kapton, it can be then used as both pulling and pushing mechanism for motor-driven SLL stiffness modulation and will be further discussed in Chapter 4.

Table 1: Material list for SLL fabrication

Materials	Young's Modulus	thickness
FR-4	$19*10^9$ Pa	0.005-0.025''
Kapton	$2.5*10^6$ Pa	0.0005-0.002''
Mylar	$1.99*10^8$ Pa	0.006''

Copper	227000 Pa	0.003-0.005''
Steel	$200*10^9$ Pa	0.001-0.005''
Double-sided pressure sensitive adhesive (PSA)	N/A	3μm

3.2 Overview of the lamination process and laser cutting technology for SLL

Our approach to the fabrication of SLLs is based on inexpensive, easily fabricated lamination process assisted by laser cutting technology. As mentioned in the conceptual designs, structural layers (FR-4, 0.005-0.020"), compliant films (Kapton, 0.5-2mils), adhesive layers (double-sided pressure-sensitive-adhesive films, 0.1 mils) and boundary layers (either Scotch tape or the combination of both compliant and adhesive films) are necessary for the fabrication of multi-stiffness SLLs' structure. Each layer is designed with its own beam profile to achieve periodical stiffness patterning in one layered laminate (figure 3.1(a)).

The individual lamination for one layered laminate combines laser cutting (UNIVERSAL LASER SYS.), aligning (dole pins) and adhesive bonding (hydraulic press), which is then divided into 4 consecutive steps, individual cuts, aligning, final cuts and release (figure 3.1(b)) First, we cut all composing layers (the structural/adhesive/compliant) with stiffness patterning and alignment holes. To form an easy sliding mechanism, two compliant films are applied on the outside of the laminate for smooth sliding interface. We then align all the individual layers using dole pins and bond them using hydraulic pressing machine. The final cut of the laminated layer is done by aligning the laser head with each corner of the piece and cut with a higher power density.

Note that double sided compliant films might cause buckling effects, we used extreme soft (Kapton 0.0010") films where buckling does not affect the bending performance of the SLLs.

Following the same steps in the individual lamination, we prepared all three composing laminates with same stiffness patterning. To fix the motion of the outer laminates, two layer-boundaries need to be poised on the sides to generate a continuous bending motion. We then insert the central layer into the SLLs' case with slidable layer configurations for stiffness modulations (figure 3.1(c)).

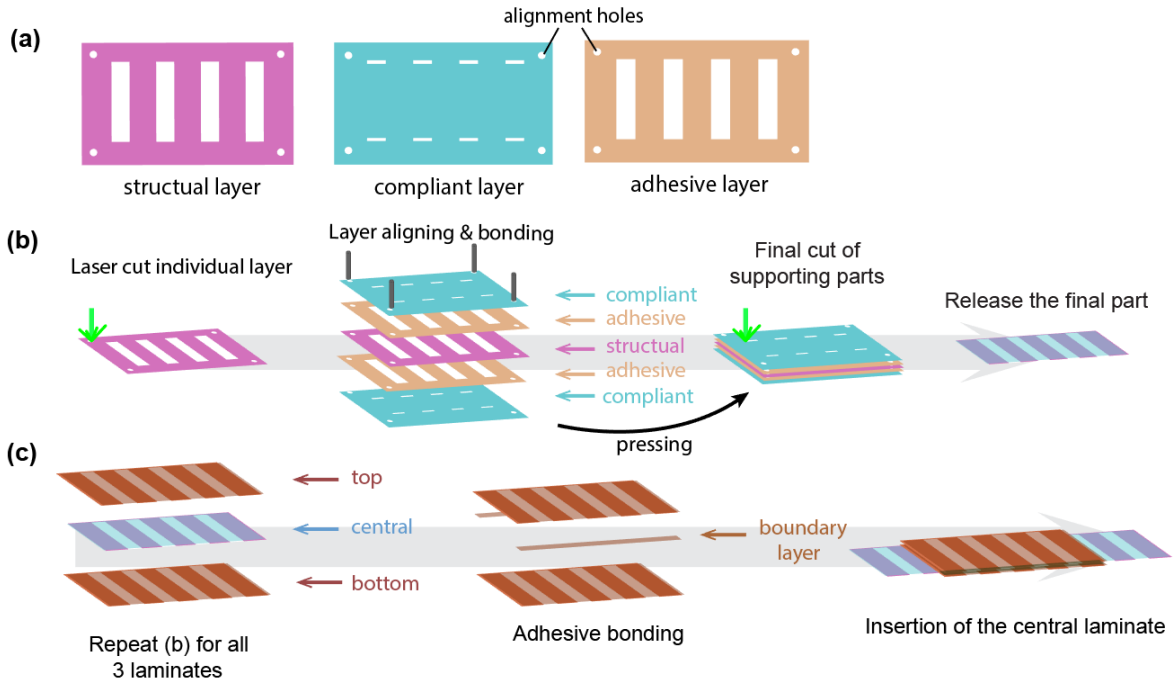

Figure 3.1 The fabrication procedures for making SLLs based on lamination and laser cutting technology. (a) the design profiles for each composing layer (CAD drawing and laser cutting) (a) The fabrication steps for making one laminated layer. (b) The lamination process for making SLLs structure.

3.3 Demonstration of one SLL prototype fabrication

The laser cutting fabrication is done by using the laser system at Prof. Tolley's lab (figure 3.2). Here we give an example of the fabrication of one SLL prototype based on the lamination process in section 3.3. First, we design the beam patterns for each individual layer in the CAD software (AutoCAD 2016). Two design principles should be carefully followed: one is the consistent design patterns of the individual layer and the final layer cut; the other one is the alignment holes located at each corner which should be exactly overlapped on each layer as shown in figure 3.3(1). We then prepare the raw materials (FR-4, Kapton and adhesive rolls), and hydraulic press the FR-4 and the adhesives to save the cutting steps for both two. The cutting process is done by using the laser cutting system from Prof. Tolley's lab (UNIVERSAL® Laser System). Based on the material cut, we can either choose CO2 laser core or Fiber core for either general cuts or metals (steel and coppers ranging from 1mil-5mils). The difference lies in the laser energy and frequency that can be absorbed by the material, which will lead to either nice cuts or uncut material with burned edges. For steels and coppers, we use the fiber core and change the laser setups as Waveform 2, 150kHz, with 2.0mW HPDFO (high power density) lens. For FR-4 and other compliant films, we used CO_2 laser core with 2.0mW lens. For materials with different thickness, we change the focal plane (the Z-axis) and tested for the best cutting parameters. We repeat the first step for each individual layer with different patterns. After the cut for all composing layers (not laminated layers), we used pins to align them as shown in figure 3.3 (6) and press them using adhesive rolls or hydraulic press depending on the thickness of the combined laminate. The final integration of the SLL is important in the sense of alignment and boundary layers preparation. Before we release the final part from the supported materials of the combined piece, we aligned the laser head with all four corners of the final piece to make sure the accuracy of the released laminates. The boundary layers are usually composed by both adhesive and compliant films and

cut in thin strips as to contribute to very little of the bending stiffness. The boundaries are also capable of ensuring continuous bending curvatures of the three composing laminates and make sure the change of alignments will generate different bending stiffness as shown in figure 3.4. We then bond the top and bottom laminated layers as prepared in the previous steps to form a SLL case. The central layer can then be inserted into the case and a final version of the SLL is shown in figure 3.3(11).

Figure 3.2 The UNIVERSAL® laser system for SLL fabrication from Prof. Tolley's lab.

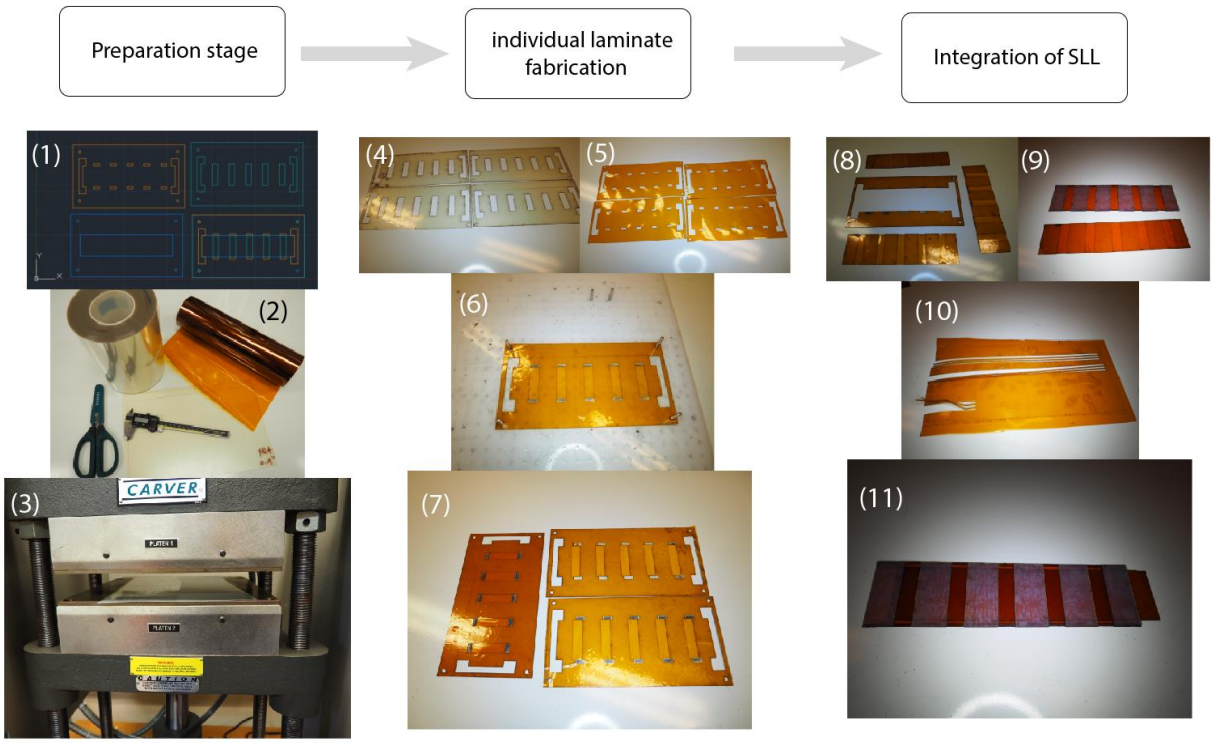

Figure 3.3 Demonstration of fabricating one SLL prototype with 24mm SLL unit's length, 36mm beam width, 60% aspect ratio made up of 0.01'' FR-4 and 200HN (2mil) Kapton films. The preparation stage includes (1) SLL design files, (2) raw materials and the (3) pressing for both adhesive and rigid parts, which shortens the cuts for both rigid and adhesive sheets for one cut. The individual laminate fabrication focuses mainly on the alignment of (4) multiple composing layers into one laminate using (5) pin aligning and (6) hydraulic pressing. 3. The integration of SLL is based on (8) (9) the final cut of each individual laminated layer. With the help of (10) boundary layers (as thin strips composed by both compliant and adhesive layers shown in the middle), the top and bottom laminated layers can then be bonded together using the boundaries to form a SLL case for the central layer to slide in between. (11) shows the final version of one SLL prototype.

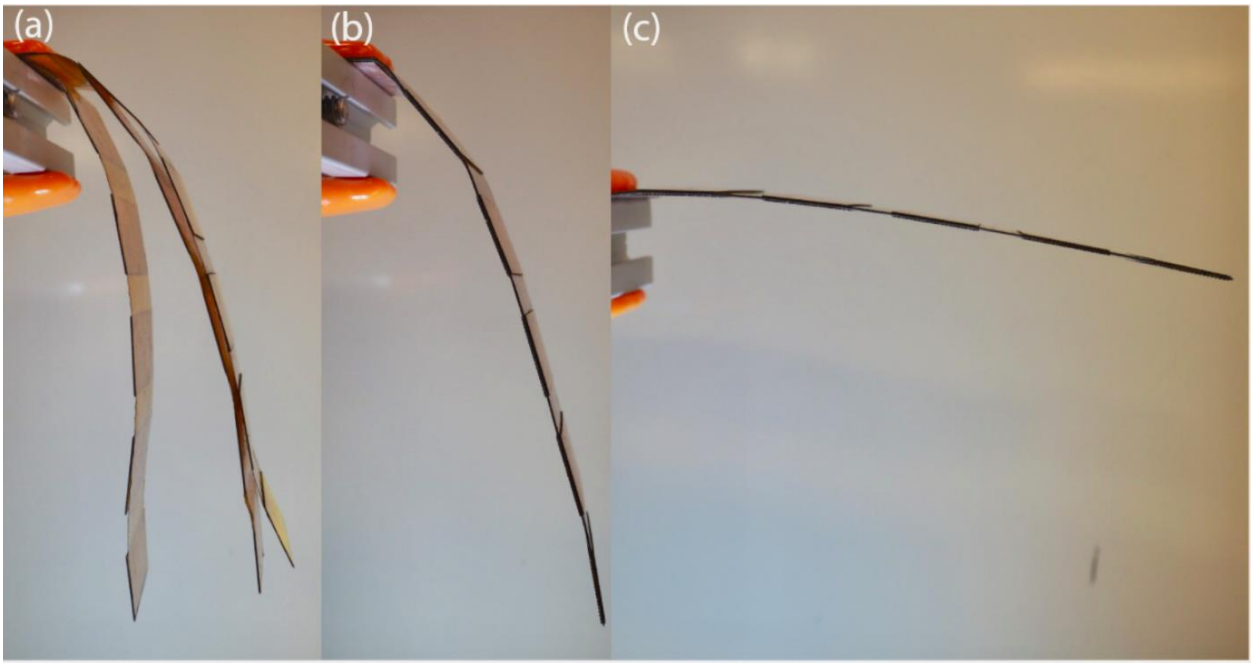

Figure 3.4 Comparison between the bending performances of one SLL prototype with and without the boundary layers (a) SLL without boundary layers (b) SLL with boundary layers in soft state (c) SLL with boundary layers in stiff state

3.4 Summary

This chapter focuses on the SLL fabrication process including both lamination and laser cutting technologies. Thanks to the laser cutting machine provided by Prof. Tolley, each individual layer can be cut with great accuracies as pre-designed and bonded together using adhesives. The lamination process relies on the precise alignment of each layer which is guaranteed by the pin alignments. By using the boundary layers as constraints on each side of the SLL, the bending motion is continuous with all three laminates bending in the same curvature. The example fabrication given in this section exploited the smooth sliding surface of the compliant Kapton films coated between the interfaces of each laminated layer which is useful for motor-driven SLL with a sliding mechanism. In a word, the laser-cutting aided lamination process is the foundation for variable stiffness SLL fabrication.

Chapter 4.

Experimental Testing and Results

The modelling of SLL in the previous section focused on a long beam consisting of 100 beam units which can be extended for different scales and applications. In this section, the SLL we made for experimental testing focused only on one beam unit to validate the theoretical models as well as measuring the stiffness change under different layer configurations within one SLL unit. Specifically, we are measuring the SLL bending stiffness from two perspectives: one is the change of the flexural rigidities from both the soft and rigid regions; the other one is the change of aspect ratios of each laminated layer. These two aspects aim to reveal different bending performances of the SLL manipulated by the design principles and further present the concept of graded and binary SLL which serve differently for stiffness modulation.

4.1 Experimental setups for beam stiffness testing

The bending stiffness of SLL is tested under the fixed end cantilever beam test. Figure 4.1 shows the diagram of the experimental rig for the SLL bending stiffness testing. In the figure, the right-hand side demonstrates the fixed end cantilever beam testing setup. With the load cell (100g micro load cell by Phidgets) fixed on a stage which is also fixed to the ground, the SLL is then pushing against the load cell under the constrained motion by the motorized linearly translational

stage (Thorlabs). The effective spring stiffness can be defined as the change of load cell reads divided by the change of translational distance by the linear stage. The motor driven system is composed by a stepper motor (Oriental Motor, PK546PMB), a driven board (Oriental Motor, CRD5107P) and an Arduino Mega2560 as an interface for giving commands to the driver board from the computer. To measure the rotational angle displacements from the motor, we used an encoder (US Digital, E5 optical kit encoder) and a LabJack U3 for data acquisition. We then translate the rotational angle change to the linear distance based on the micrometer mounted on the linear stage. In this setup, we exploited an easy method in achieving miniature linear translation by using a coupler and a flexible cable (SDP/SI, remote control flexible shafts) connected with the micrometer of the stage. Such a low-cost design is inspired from [38] and proved to be useful by many others. The reads from the load cell is received by the computer through HX711 (load cell amplifier) and an Arduino Mega2560 board, which is further converted to Newton forces after several calibrations. Figure 4.2 (a) shows the experimental setups for the beam testing stage. Figure 4.2 (b) demonstrates the setups for using stepper motor in creating linear motions in the linear stage using flexible coupling.

Note that in this experiment, we focus on forces generated by miniature beam deflection to make sure the results follow Euler-Bernoulli beam theory. For each test, we change the configurations of the SLL by hand but keeps the exact fixing point and testing point of the beam's tip.

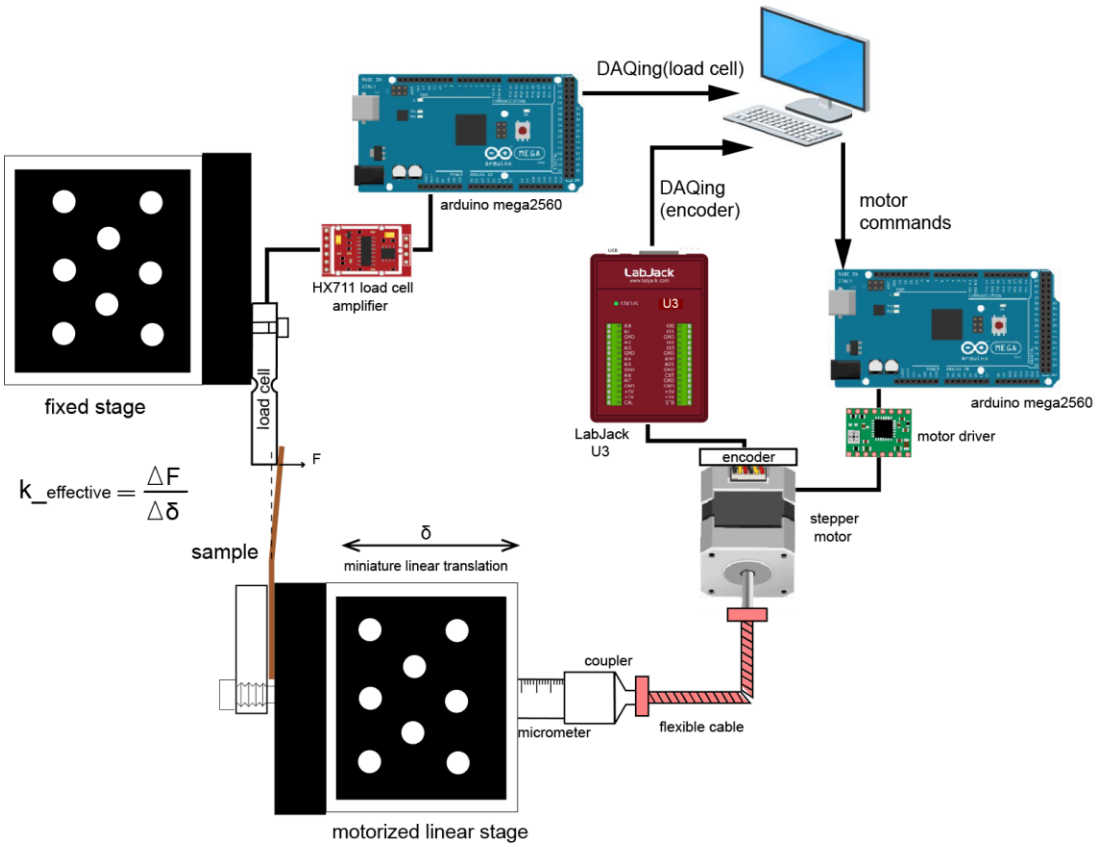

Figure 4.1 The experimental rig for SLL bending stiffness testing (all the black lines between each module represent electrical wirings).

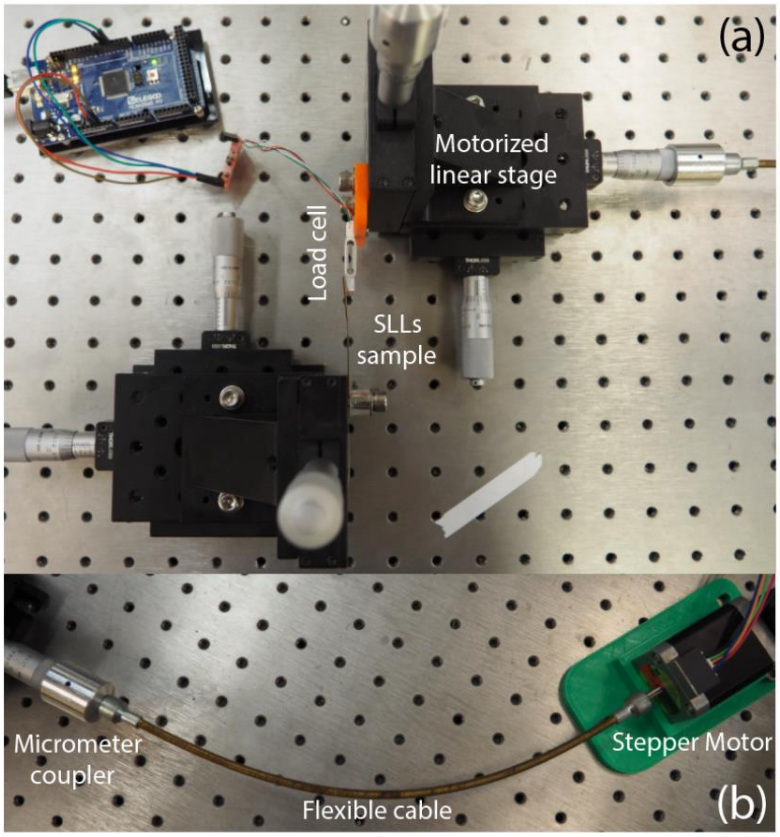

Figure 4.2 Experimental setups for SLLs bending stiffness tests (a) Cantilever beam bending stiffness measured using SLLs specimen (one beam unit) fixed on a stationary stage with the load cell on a motorized linear stage. (b) Connection between a stepper motor and the motorized linear stage using flexible coupling (a flexible cable with a machined coupler).

4.2 Variable stiffness under changing E_rI_r and E_sI_s

As predicted by the modelling, changing E_rI_r will significantly affect the stiffness of the SLL in the stiff states with little influence on the soft state's stiffness; whilst changing E_sI_s will change the stiffness in the soft states with little modulation of the stiff state. Therefore, the expectation in this test is to separately control the stiffness in the stiff and soft state by changing the beam flexural rigidities in different regions and thus manipulate the potential range of the stiffness variations.

For the specific testing method, we are aiming at testifying just one SLL unit and changed the configurations between different aligning states as previously described. By testing one SLL, the beam bending motion can be controlled in a miniature range (since the soft state will be too soft for beam testing) even in the softest state. In this section, we are going to test the bending stiffness by changing the flexural rigidities of both soft and rigid regions of the composing laminated layers of SLL.

The way we manipulate the flexural rigidities of both soft and rigid regions is based on the change of the design width of the laminate's top view profile, which indirectly changes the effective 2nd moment of area of the beam along the longitudinal direction and thus the EI profile would be changed. Figure 4.3 clarifies the strategy used for multiple E_rI_r and E_sI_s preparation for the testing of changing flexural rigidities.

For the testing sample, we used FR-4 (0.01 inches) and Kapton (1mil) as our main materials. The outer case is made of both FR-4 and Kapton as shown in figure 4.4. The Kapton film is the only component for the soft regions of the outer layers serves as a low-friction sliding interface. The central layer is composed by only FR-4 sheets with a change of the flexural rigidity of the soft region (E_sI_s) by changing the beam width of the soft region. The effective beam length for the bending motion is 40mm. The beam width of the outer and central layers is the key for changing the E_rI_r with a selection of 40mm, 30mm and 20mm. Based on this, we can then choose one outer layer set, and change the central layer to vary the flexural rigidity of soft regions, where the E_sI_s change is only determined by the central layer, with the E_sI_s of the outer layers unchanged. On the other hand, by choosing the same beam width of the soft region with different beam width of the rigid regions of the central layer, we can compare the stiffness of SLL with different E_rI_r but with

the same E_sI_s. The goal of this experiment is to control the flexural rigidity of either the soft regions or the rigid regions to vary the stiffness of the softest state and stiffest state separately.

Figure 4.4 shows the change of stiffness in both soft and stiff state with the modulation of E_rI_r and E_sI_s. Figures in the first row shows that the increased E_sI_s will increase the stiffness in the soft state as predicted by the model whilst maintaining the stiffness in the stiff state. Among different E_rI_r sets, such a trend can be observed. On the other hand, figures in the second row shows that by increasing ErIr with the same EsIs for different outer layers, we can always observe a trend of significant change of bending stiffness in the stiff state, but relatively little increase in the soft state as predicted by the model. According to the results, the predicted model matches well with the testing data with discrepancy in cases, where the overall bending stiffness of the SLL is below a certain point (100N/m). In these cases, the bending stiffness will be higher than the predicted stiffness, which can be explained by the jamming or frictional effects of the SLL from the 3D geometrical features. The jamming effects will increase the bending stiffness however cannot be accounted for by the modelling.

Therefore, by changing the flexural rigidities (materials) of the soft and rigid regions, we can manipulate the potential range of the stiffness change from the soft state to the stiff state of a SLL prototype. Most importantly, the stiffness change range can be tuned by either only the softest state and the stiffest state, which provides a theoretically infinite stiffness change range for different applicational areas. Such a design principle reveals the fundamental feature of a multi-stiffness laminate composed by materials with different flexural rigidities.

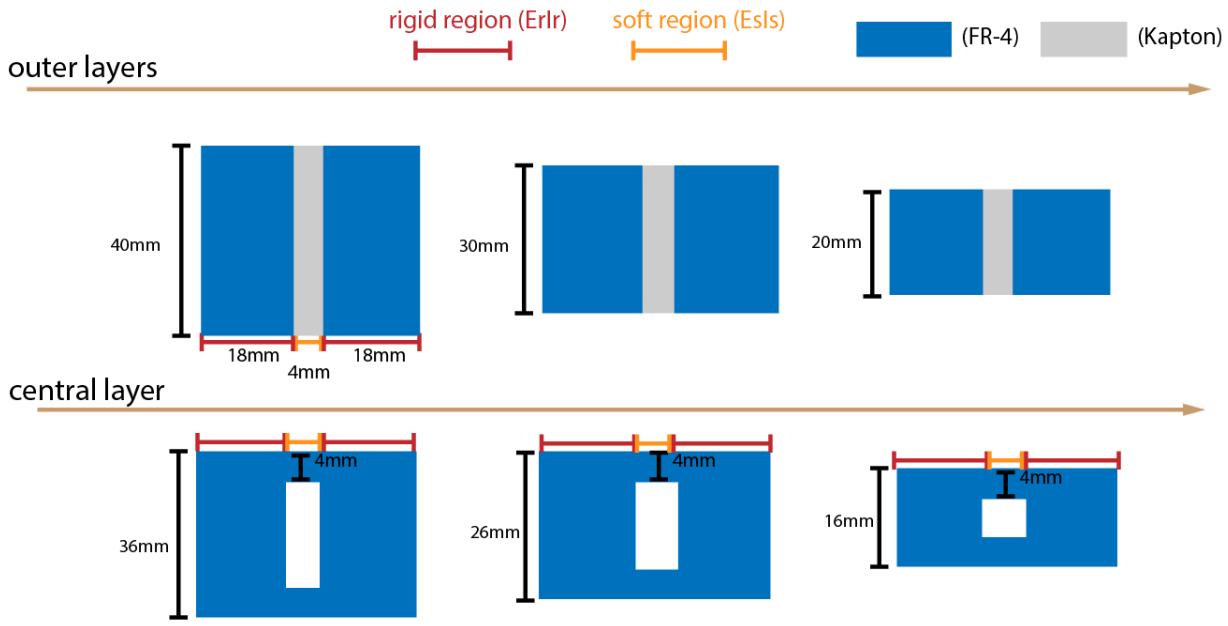

Figure 4.3 Testing samples used for changing E_rI_r and E_sI_s (longitudinal beam profiles).

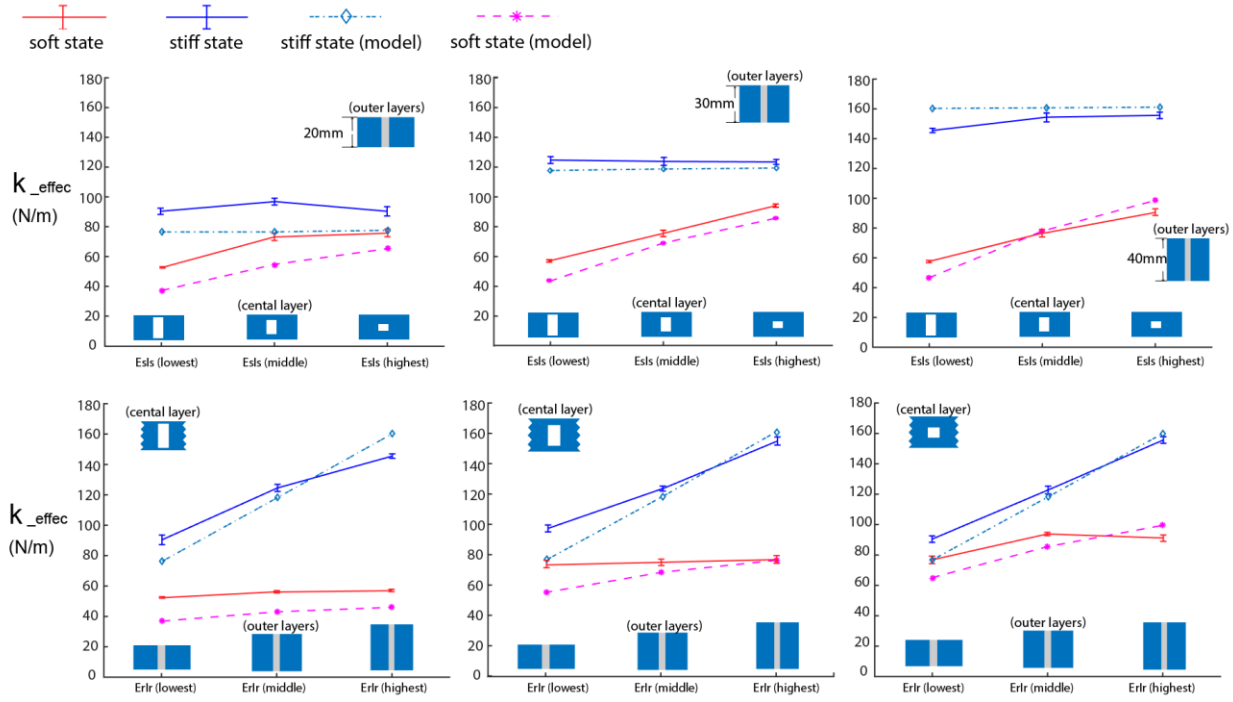

Figure 4.4 The experimental data and predicted stiffness of the SLL in both soft state and stiff state with the change of E_rI_r and E_sI_s. The figures in the first row is the comparison between different stiffness with only changes of E_sI_s. The second row is the comparison between SLL's stiffness with only changes of E_rI_r.

4.3 Variable stiffness under changing aspect ratios

The change of aspect ratios is an important design principle since it determines the overlapping regions of each laminated layer in the SLL during the stiff state. For instance, since each laminated is made up both soft and rigid regions, the overlapped rigid parts will form a strong bending performance until the alignment changes to the soft state.

The testing samples are fabricated using following the same rules (FR-4 0.01 inches, Kapton 1mil) in the previous section, with the outer layers composed by both Kapton and FR-4 and the central layer composed by only FR-4. We then choose a fixed ErIr and EsIs design with a series of changes of the aspect ratios between each test, ranging from 50%-90%.

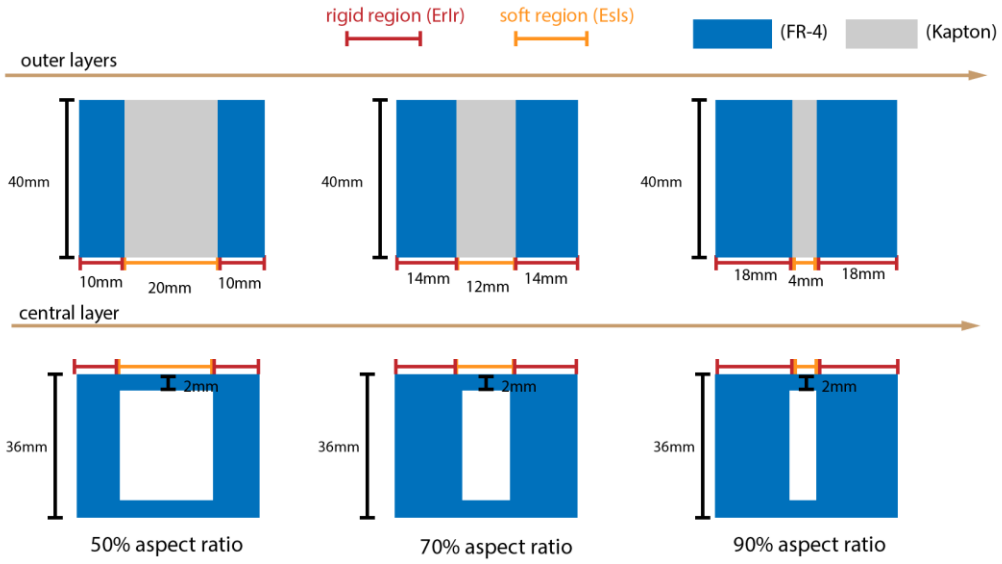

Figure 4.5 Testing samples used for changing aspect ratios (longitudinal beam profiles). The examples shown here are SLLs with 50%, 70% and 90% aspect ratios.

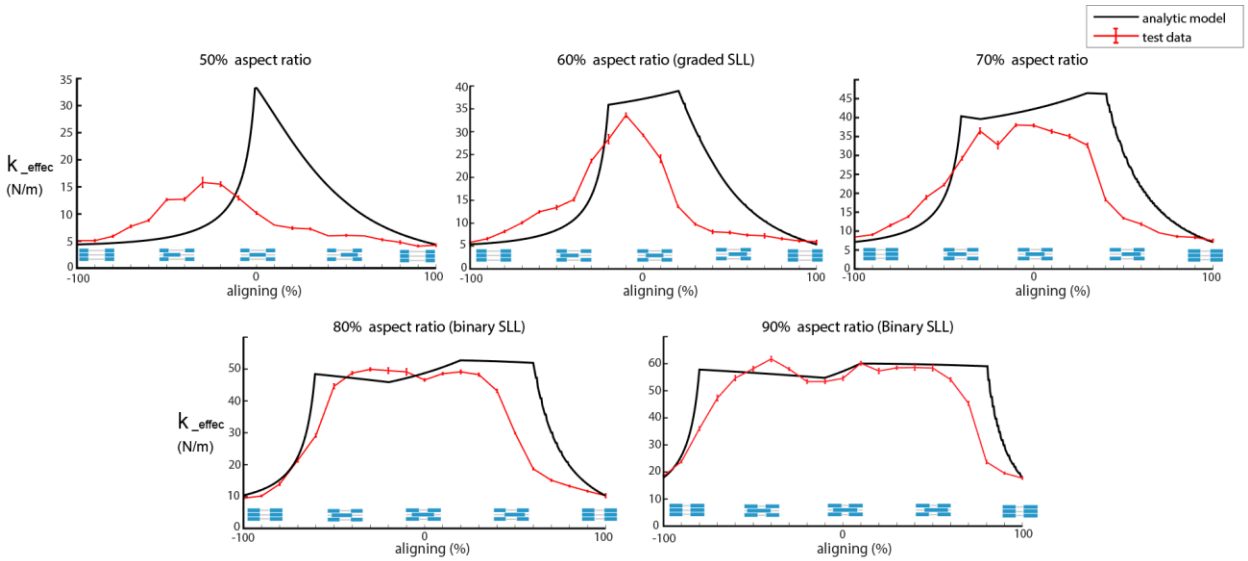

Figure 4.6 Comparisons between the experimental data and predicted stiffness of the SLL along all the alignments with changing aspect ratios (The experimental data is collected for every 10% change of aligning percentage). The aspect ratio ranges from 50% to 90%. The diagrams show the alignment of different states with the blue representing the rigid regions and the grey for the soft regions.

Figure 4.7 Segmented bending curvature of SLL due to non-overlapping rigid regions in the stiffest state (SLL with aspect ratio 50%).

4.3.1 Binary and graded SLL with different aspect ratios

In figure 4.4, each figure exhibits the stiffness-alignment curvature under different aspect ratios of the testing SLL. With increasing aspect ratios, the stiffness for all the aligning states are raised by as much as three folds; on the other hand, the SLL' stiffness stays in the on-state (stiff

state) longer as we increase the aspect ratios, meaning that even as the SLL's alignment state is changing, most part of the sliding motion will exhibit a high stiffness bending performance. Such a feature is shown by the testing data as well as the predicted model, with the model overestimating the tests in the lower aspect ratios. The discrepancy can be due to the geometrical design of the SLL, where low aspect ratio SLL does not have enough overlapping areas between the rigid regions of the laminated layers that lead to discontinuous bending curvature shown in figure 4.5.

On the other hand, the variable stiffness curvature can be divided into two categories: one is the graded SLL where the stiffness gradually varies with the peak stiffness found only within a confined range (aligning percentage from -10% to 10%). The other one is the binary SLL where the stiffness of the beam stays in the off-state (soft state) within a confined range and keeps in the on-state for most of the sliding motion, the transition between soft and stiff state is shorter than the case in the graded SLL. Based on their different stiffness modulations, the binary SLL can be used in areas where the variable stiffness is desired for an on-off pattern with the on-state stiffness as high as possible. Since the transition between the on to off state is shorter, the requirement for the actuation source can be lowered with less energy (actuation distance) consumption. In the meanwhile, the graded SLL would be beneficial in cases where the stiffness needs to be gradually changed as a response for continuously changing working environments. Since the transition from a soft state to a stiff state is relatively longer, the requirements for the exact position control of the central layer is higher in the graded SLL.

4.4 Summary

In this chapter, we provide a low-cost, motorized linear stage system for the testing of beam bending stiffness. The test of the SLL variable stiffness is based on one SLL unit with the change of two design principles, the flexural rigidities of the composing regions and the aspect ratios. The

change of the ErIr/EsIs are mostly reflected by the potential stiffness range and limits a SLL could modulate. The change of aspect ratios will manipulate the stiffness-alignment curvature in both the effective spring stiffness and the stiffness transition process, which can be further divided into binary and graded SLL for different stiffness modulation and applications. In the future section, the SLL would be implemented into different scenarios as a proof of its multi-functionalities as an appendage or building blocks for future robotics.

Chapter 5.

Experimental demonstrations of SLLs

Variable compliance is one of the most desired properties for future robotics in achieving multi-functionalities to negotiate with changing environments and working conditions. In nature, animals with variable stiffness in their muscles can generate an infinite variety of behaviors with great efficiencies. Such a feature inspires engineers to create robots with stiffness modulation over a range of multi-stiffness. The changing mechanism for such a variable compliance is essential in as regard to the fabrication scales and energy portability. In this chapter, we are going to demonstrate how SLL's multi-stiffness is being actively controlled and further implemented into different scenarios for an improved performance.

5.1 Variable compliance SLLs as a wing structure

SLL, based on its variable stiffness along its longitudinal direction, can be implemented as a variable stiffness or morphology control surface in the engineering area of aerodynamics. In this section we used wind tunnel (figure 5.1) to demonstrate the change of both stiffness and morphology of the SLL in a constant air flow condition.

Specifically, the SLL is mounted on a fixed frame composed by 8020s, which is then fixed inside the wind tunnel. The motorized linear stage serves as the actuation source for the SLL's

sliding layer configuration, which is repeatable for both pushing and pulling of the central laminated layer. We then repeated the sliding motion of the motorized stage to be between the stiffest and softest state of the SLL (which is half the distance of a SLL unit) and measured the tip displacement of the SLL as a demonstration of the variable compliance transitions in an aerodynamical environment.

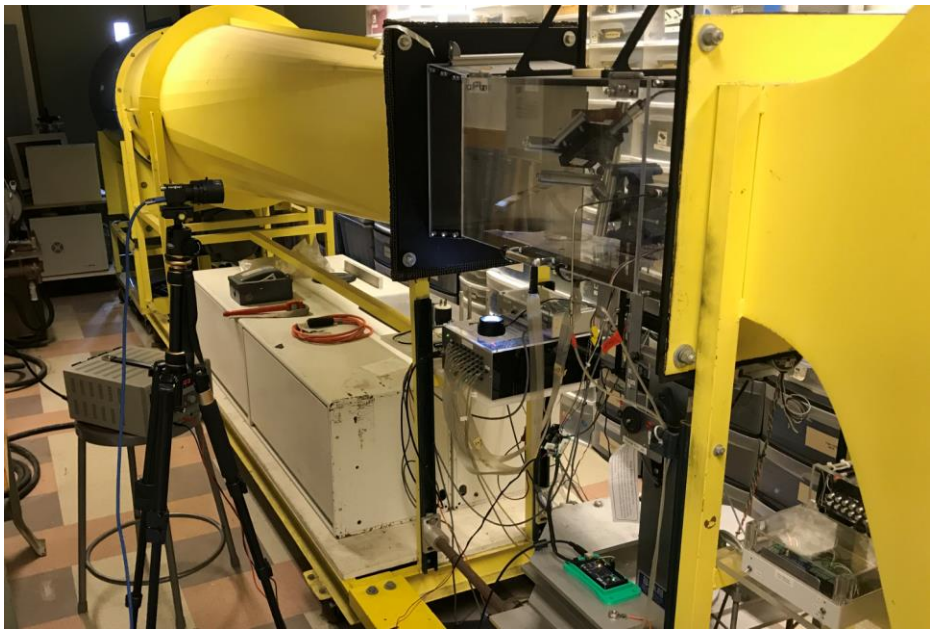

Figure 5.1 Wing tunnel from the wind tunnel laboratory of UCSD.

Figure 5.2 A long SLL prototype used for wind tunnel testing

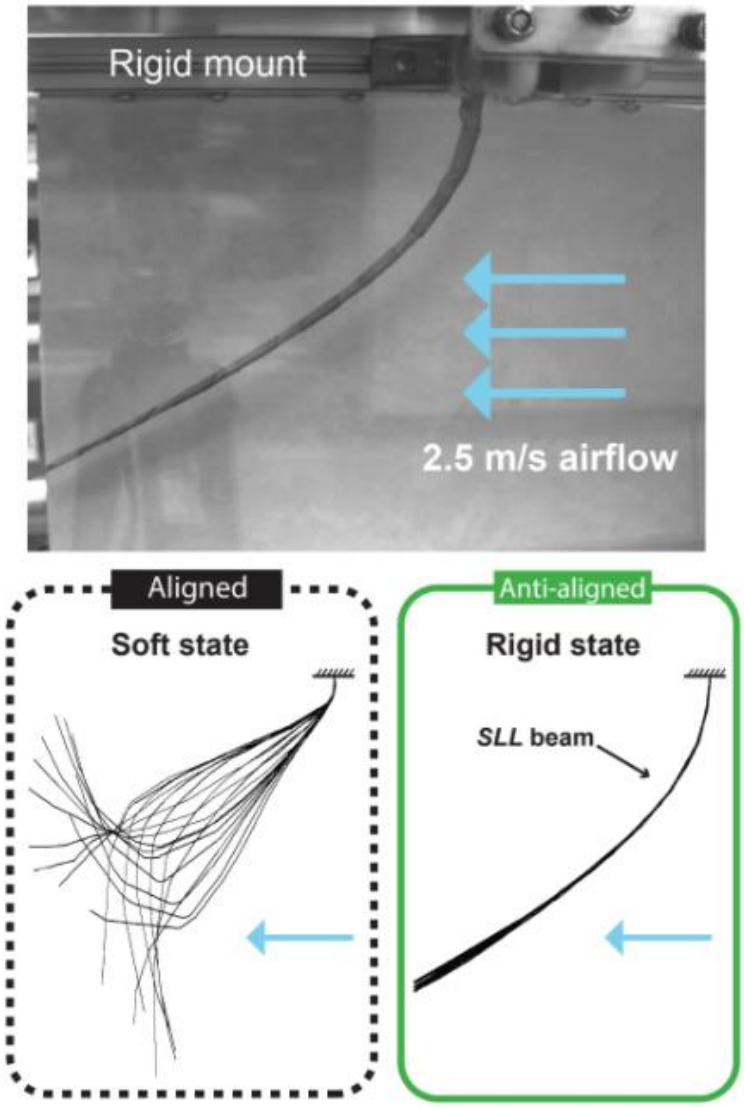

Figure 5.3 Beam profiles of SLL fluttering in wind tunnel in two different stiffness states with a constant air speed at 2.5m/s (preliminary test of SLL variable compliance). The snapshots are taken over 10 seconds for every 0.5 seconds.

In the preliminary test of SLL variable compliance, we fixed the SLL and tuned the layer alignment by hand to see if the variable compliant behaviors activated by the air flows. In figure 5.3, the two different states will form different flapping profiles at the same air speed. In the soft state, the bending curvature has several nodes and is unstable during the record time. To compare, the SLL in the stiff state will bending in a continuous curvature with little change of the

geometrical shape, showing its stiffened rigidity against the constant air flow. The morphology change is increased with a random pattern in the soft state, corresponding to certain mode of the beam fluttering.

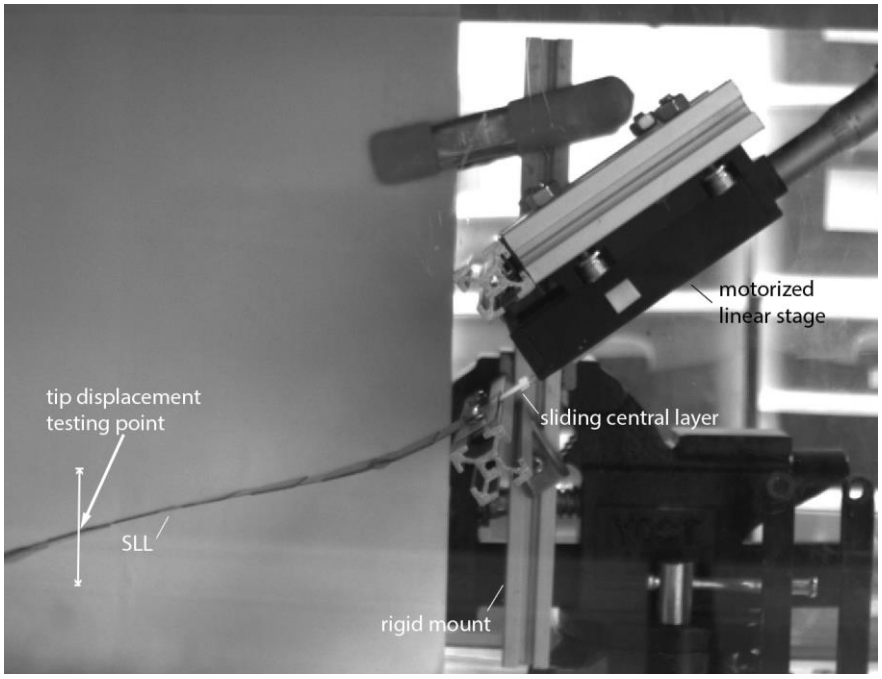

Figure 5.4 The experimental setups for an active control of SLL's variable compliance in a wind tunnel. The motorized linear stage is driven by a stepper motor through a flexible shaft and machined coupler as described in Chapter 4. A tip displacement is measured as indicated in the picture.

Based on the previous test of SLL different fluttering motions in the wind tunnel. We then implement a motorized linear stage as an actuation source for the SLL active stiffness control as shown in figure 5.4. We used vision camera to record the tip position as a demonstration of the flexibilities of the SLL under the air flow. Figure 5.5 demonstrates the different tip position the SLL undergoes with the motorized sliding motion of the central layer (presented as aligning percentage of the layer configuration).

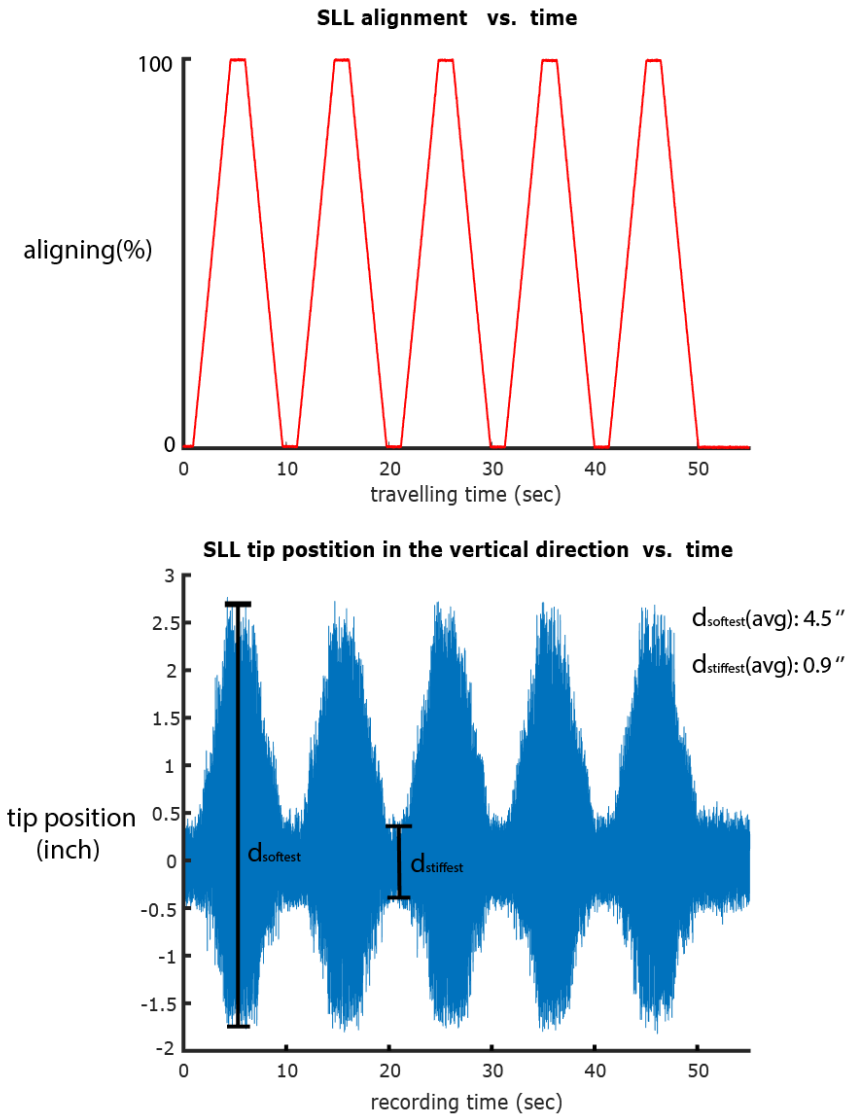

Figure 5.5 Changing SLL alignment using motorized stage at a constant speed pattern (top) and the corresponding tip position change of the fluttering SLL under the same sliding motion in the wind tunnel (bottom).

In the demonstration, the testing point selected is one of the points that amplify the most difference of tip displacements between the soft and rigid state. In the soft state, the SLL's tip displacement is about 4 folds of the results in the stiff state. Such a result reflects the difference of morphology changing abilities as well as the variable stiffness of a SLL prototype, which could be

driven external actuation source in a real-time control pattern. In test, the stiffness changing speed is tuned for video record but could be increased for rapid stiffness modulations.

Based on its variable flapping behaviors in the wind tunnel, the SLL can then be implemented as a morphing wing structure or hinge appendage capable of generating different shapes and displacements during the flight. For instance, the soft state can be used as a morphable and flexible wing structure for high amplitude flapping motions and the stiff state can be used for gliding motion where the wing structure will maintain as a flattened plate with a camber shaped wing profile for the air to circulate around the wing. As to achieve different aerodynamical performances as a flapping wing material, the SLL can be swapped between stiff and soft state using an embedded actuation source, such as PZT actuators and micro linear servo motors, to meet with different flying conditions. The future applications for variable compliance flapping wings can be expanded with the development of smart and integrated stiffness changing mechanisms.

5.2 Variable compliance SLLs as a robotic fish tail

Fishes use fins to as a general-purpose device to locomote in the fluid environment. The rayed structure of the fin is found to be the main reason for the versatility of fish aquatic locomotion among 99% of all living fish species [39]. For either stationary holds in a turbulent flow or a burst of motion, the fins are all being widely exploited and manipulated to meet with the changing aquatic conditions. In the meanwhile, the mechanical stiffness of the fin is the key parameter that affects its propulsive performances, and has been proved to have many important influences on the fish (robotic fish) aquatic behaviors by both biology and robotics [40][41].

In this demonstration, we fabricated SLL with as a fin-like composite beam with hexagonal patterns of the rigid regions on the outer layers. The inner layer is still in a rectangular pattern with

the with the same geometrical length of l_{rigid} and l_{soft} as with the outer layers, as shown in figure 5.5. The SLL is then mounted onto an acrylic frame, which is mounted onto the rotor shaft of a stepper motor as to generate the pitching motions of the SLL (robotic tail). As the flapping motion is generated by the pitching motion of the motor, which will cause yaw motion of the car, we build tracks using acrylics and 8020s to constrain the motion in the forward direction. Since the pitching motion will generate yaw motions and torques, the tracks can also reduce the oscillation of the whole moving system and the errors sensed by the load cell (the load cell is sensitive to the normal stress but can also sense force stress and from the sides). The solenoid (Guardian, 12V) acts as an actuation source that can change the sliding configurations of the SLL from the stiff state to the soft state and is controlled by a switch. The automatic control of the corresponding stiffness states helps with the transition between stiff and soft tail thrust generations without having to reconfigure the layer alignment by hand, which serves as a practical solution for stiffness modulation. Even the sliding motion is independent of the flapping motion, the layer can only be easily slid when it forms as a straight beam. The vision camera is responsible for video recording the flapping motions as well as the beam fluttering geometries under different driving conditions. We then fixed the load cell with 8020 extrusions and align it along with the moving direction of the car, so that the car will push on the load cell in the forward direction to test the thrusts generated by the flapping motion.

We measured the thrusts from the flapping SLL as a pressure force onto the load cell and recorded the force generation over 1 minute of flapping motion. Each time we start from the same place where the car is as close to the load cell as possible with no pushing on the load cell. We make sure the low-friction condition of the tracking system such that the force of the load cell will come back to zero whenever we stopped the flapping motion (Since the load cell with an acrylic

extension is very stiff). We then take the average of the force recorded during that one- minute duration and repeat this procedure 5 times to make an average as the approximation of the thrust generation in that specific driving condition. The thrust measurement is done over two different driving amplitudes and a range of different driving frequencies. The goal is to testify the usefulness of SLL's different stiffness states in generating thrusts as a robotic fish tail under different working conditions, such as open water and confined water tunnels. As to generate observable thrust forces, the SLL used in this experiment is strengthened with two layers of the FR-4 (0.013'' of each layer) on the rigid regions, the soft region of the outer layers is made of Kapton (2mil), and the boundary layers are made of three strips of Scotch tape stacked together.

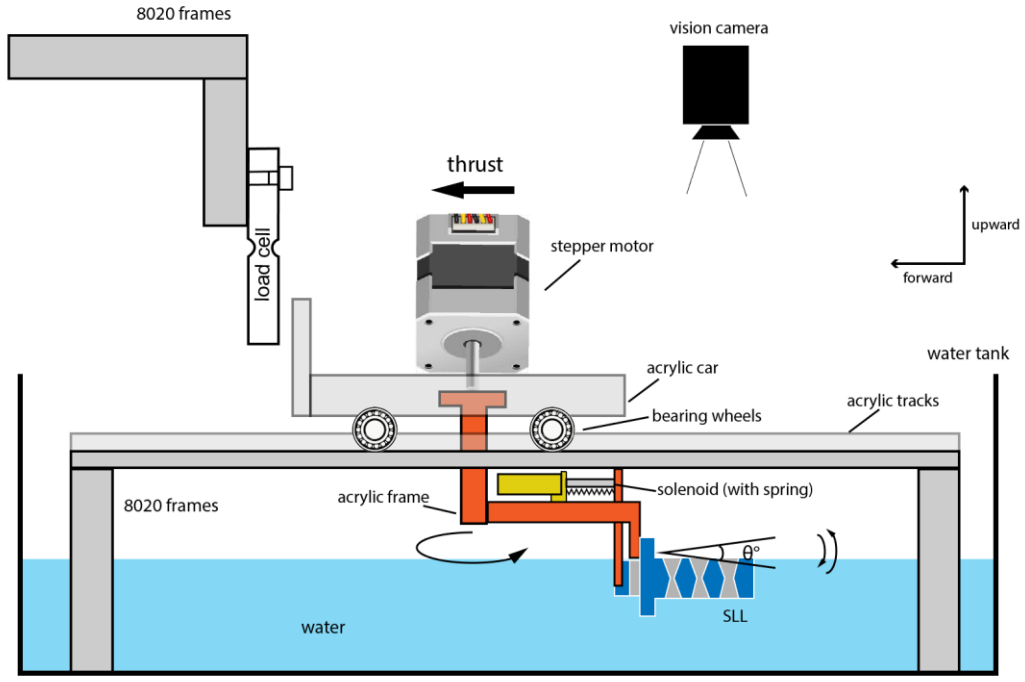

Figure 5.6 Layout of the experimental setup for thrusts measurement generated by a SLL flapping in a water tank as a robotic fish tail.

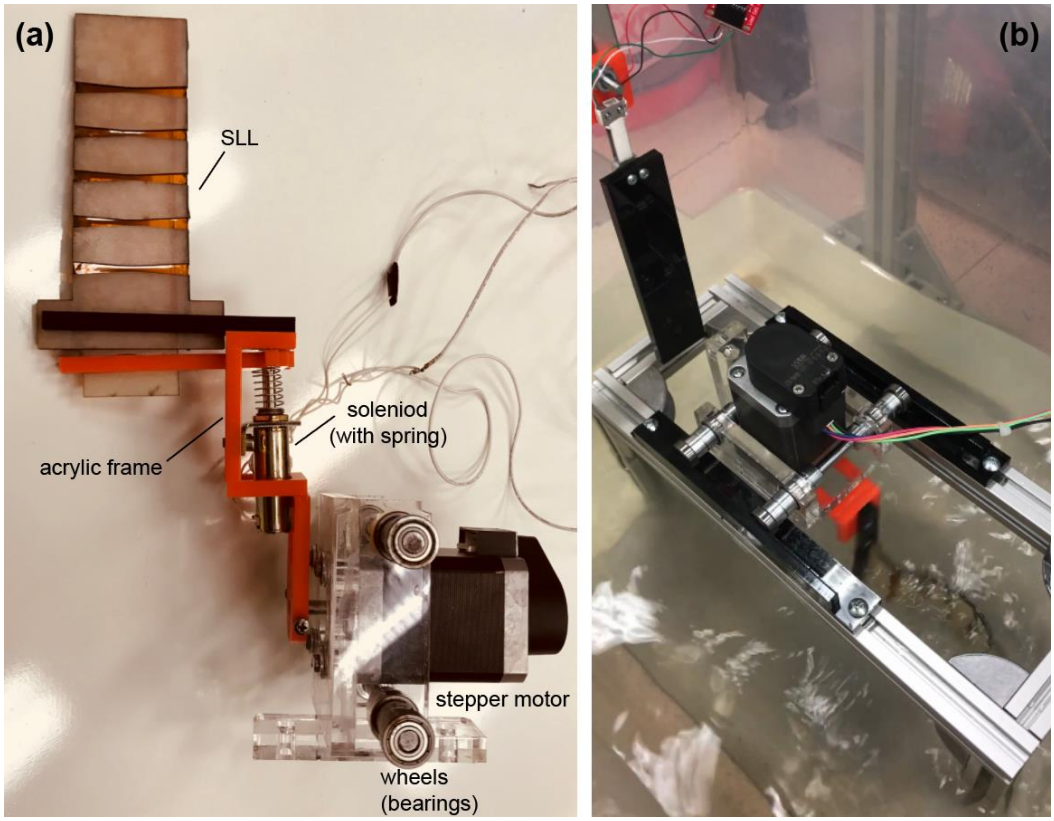

Figure 5.7 the actual design of the SLL and the swimming robot prototype.

Here I need a picture for flapping tail comparison

Figure 5.6 is a comparison of thrust generations between the stiff and soft state SLL in a low driving amplitude over a range of driving frequencies (from 2hz to 5hz). The result shows that within a lower driving amplitude, the stiff state SLL is better than the soft state SLL in thrust generation, however, less effective when we increase the driving frequency. On the contrary, the soft state SLL can be effective in thrust generation in a confined aquatic environment if driven by a high frequency. The high frequency plus a low driving amplitude can be beneficial in achieving efficient flapping curvatures of the soft state SLL than the stiff state SLL. This implies the application for changing SLL into soft state robotics fish tail if swimming in a confined space.

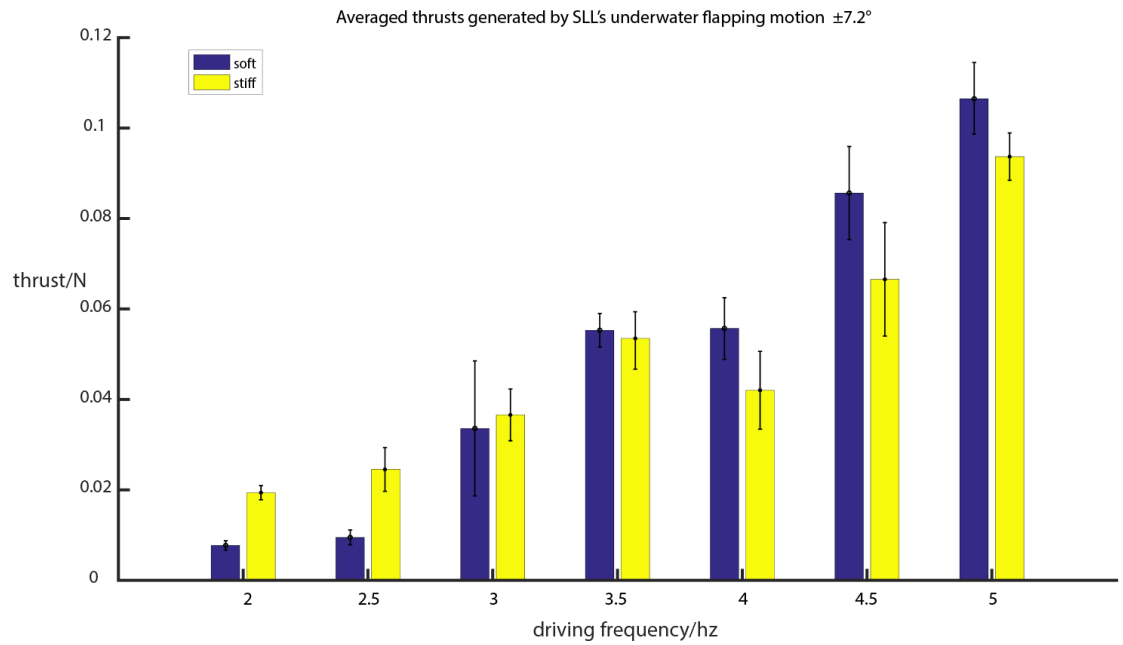

Figure 5.8 SLL's thrust comparison between soft and stiff state over a range of frequencies under flapping amplitude ±7.2° (14.4°).

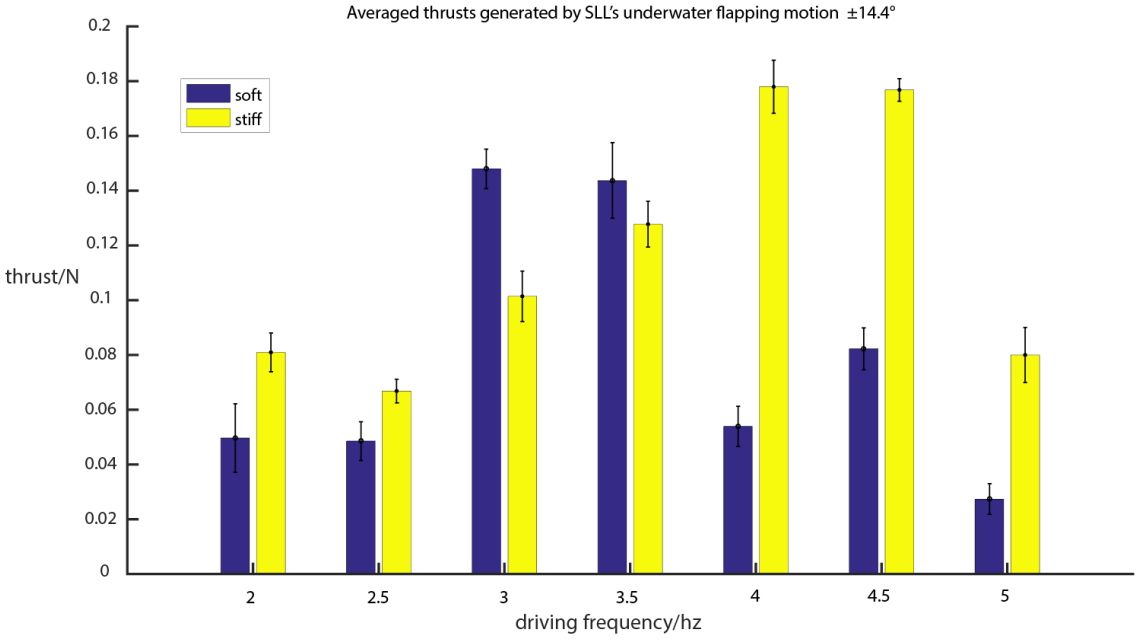

Figure 5.9 SLL's thrust comparison between soft and stiff state over a range of frequencies under flapping amplitude ±14.4° (28.8°).

Figure 5.9 is another comparison of thrust generations between the stiff and soft state SLL in a high driving amplitude over a range of driving frequencies (from 2hz to 5hz). The results exhibit two different thrust peaks for the stiff and soft state, where the stiff state SLL can be effective in thrust generation around 4hz and the soft state SLL around 3hz. Furthermore, the maximum thrust a soft state SLL can generate is comparable with the maximum thrust given by the stiff state but rather with a lower driving frequency, meaning that the energy consumption can be decreased by using the soft SLL with comparable swimming performance. All these indicate that an optimized swimming speed or force is related with the combination of driving conditions and the tail stiffness, and thus the variable stiffness SLL can be exploited for an improved swimming performance as a response to each changeable working and driving condition.

5.3 Open-water vs. Confined space undulatory swimming performances

Based on the previous measurement of the thrust generations from SLLs' passive propulsor under 2 different states, we proposed another use of variable compliance SLLs navigating through structured aquatic environments. Namely, we hypothesize that a high-frequency swimming pattern in open water would be optimized by the high-stiffness SLL state, and a slow but steady swimming pattern through a narrowed confined space would be optimized by the soft stiffness SLLs state. To demonstrate this, we exploited the same design concept by using a double-rail system with a longer SLLs as a passive propulsor (figure 5.10 (a)). In the system, 2 sliders combined with an acrylic plate consists of the base of the swimmer, where the SLLs connected with the stepper motor using a coupler to generate thrusts in the water. As a demonstration, we drove the swimming robot in both an open water scenario (in a water tank) and a narrowed channel space (45 x 392mm, with 2 acrylic plates sitting on the bottom of the tank as the walls) (figure 5.10 (b)). We then tracked positions of the tails and sliders along the rail system and observed the swimming performance.

Figure 5.11 illustrates the performances of the robotic swimmer navigating through dual-water environments. Note that a high sweeping amplitude will increase the thrust generation. We choose a high sweeping amplitude to maximize the thrust. In the open water, stiff state SLLs can generate powerful strokes with a high sweeping amplitude (±72°), which can easily navigate along the rail system (figure 5.11 (a)); however, a soft state SLLs driven with the same condition will not be efficient enough to glide through the rail system. On the other hand, as we built the walls and restricted the flapping motion of the SLLs tail, the soft state SLLs is found useful in generating low amplitude (±21.6°) steady motion through the channel whereas the stiff state can only pass through the first half of the channel as the tail's end is hitting onto the acrylic walls (figure 5.11 (b)). This can be explained by the physical interference between the two objects combined with the water reaction effects caused by the stiff SLL tails pushing water to the sides. Since more water is pushed to the sides instead of backwards, the total thrust generated is worse in this case. The results from the robotic swimmer indicate a potential application for variable stiffness passive propulsors in aquatic environments. Such a result reveals opportunity for building robots to exploit new tunable compliance materials that can maintain optimal swimming performance over a range of working conditions.

5.4 Summary

In this chapter, we demonstrate the SLL’s multi-stiffness exploited under different scenarios. We first fabricated a long SLL for the fluttering motion tested in a wind tunnel. Under the same air speed 2.5m/s, we observed significant change of wave motions and morphology changes between the stiff and soft state, indicating strong stiffness variation under the sliding configuration of the SLL driven by the actuation source. The variable stiffness is gradually changed intermediate stiffness states available and the flexibility it generated can be used as the

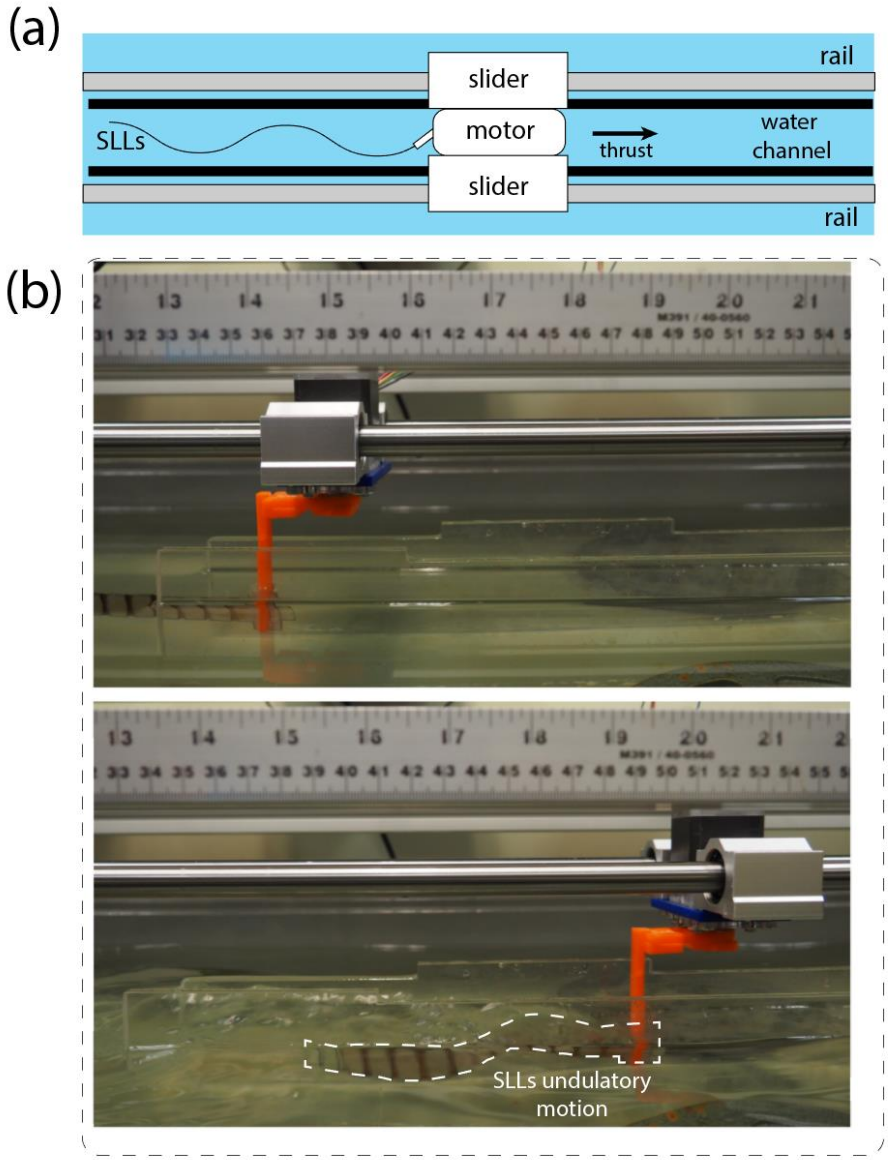

Figure 5.10 Setups for rail-based SLLs robotic swimmer (a) Diagrams of robotic swimmer swimming through a confined channel using SLLs tail from top view (b) Robotic swimmer passing through a confined channel based on undulatory motion of the SLLs propulsor (driven by a stepper motor).

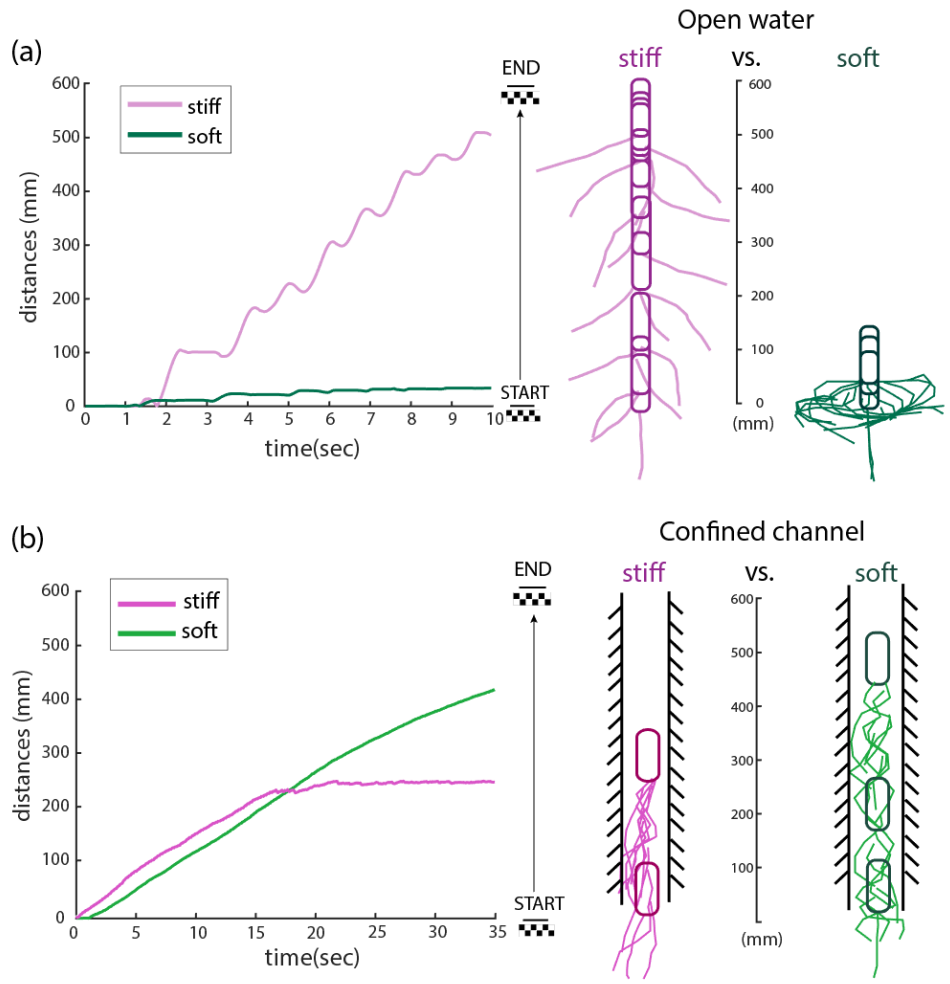

Figure 5.11 Tracking of robotic swimmer under a dual aquatic environments (a) Open-water high amplitude swimming pattern (tracking every 0.67 seconds). (b) Confined space steady speed swimming pattern (tracking every 3 seconds).

constructing appendage or building blocks for morphing wing structure, which can be tuned for the optimized flying performance in either flapping or gliding scenarios. The second demonstration is to build a robotic fish tail with a thicker and stronger SLL to generate different thrusts under different layer configurations with the flapping motion in the water. Such a robotic fish is made up by the combination of a SLL robotic tail and a car structure with low friction and constrained motions on a track system. The resulting thrusts generated by the SLL fish tail under different

stiffness states show that the swimming performance is related with both the driving conditions and the tail stiffness, and each stiffness state has its own dominant thrust generations which could be exploited under different working conditions. As a fish is swimming under a changing environment, the variable stiffness can help with the optimization of the swimming speeds and energy consumptions which on the other hand would be hardly achieved by a beam with a constant rigidity factor. The result also implies the usefulness of soft state SLL flapping in a confined space with a relatively low amplitude (less than 15°) and high driving frequencies (higher than 3hz).

Lastly, we note that in this study SLLs are beam-like structures that are uni-directionally controlled as passive propulsor elements into mobile swimming robots to generate different propulsive performances over a range of driving conditions. As a next step, we seek to target two desired robot locomotor behaviors: fast open water swimming, and steady swimming through narrow channels emulating underwater caverns and pipes. We demonstrate that real-time stiffness variation of the passive tail enables optimal thrust generation in these two locomotion modes. Hence, we believe that our SLLs strategy opens avenues for the design of new class of robotic material enabling robust and adapatble undulatory locomotors that can travel through complex environments for search and rescue, exploration and inspection operations, environmental monitoring, and medical procedures.

Chapter 6.

The Extensions of SLLs Concept

Inspired by the dual-stiffness structure, the SLL with a sliding layer mechanism can generate multi-stiffness for multi-functional robotic applications. In the previous sections, the SLLs are all made by elastic materials (FR-4 and Kapton) under lamination process and laser cutting technologies. However, the fabrication approaches are not limited within the lamination process. Such a multi-stiffness structure can be made with other manufacturing techniques and the material composition can be changed by materials with ductility and viscoelasticity for a combination of different variable properties. In this chapter, we are going to explore different fabrication approaches for the same SLL concept as an extension for its potential applications multiple areas.

6.1 3D printed SLLs

A simplified SLL fabrication can be achieved by using 3D printing technology (figure 6.1). Without the lamination process and pattern designs for each layer, the 3D printed SLL can be fabricated at one time and assembled using the hinge structure on without extra adhesive or connecting parts, such as bolts and nuts. In this section, we demonstrated a practical way of designing 3D printed SLL in a larger scale with a chain-shaped geometry.

Basically, a 3D printed SLL is composed by periodic sections linked by hinge structures as shown in figure 6.1. The two units are composed by rigid 3D printing materials (PLA), with two connection heads (male and female connector) on each side of the unit. Therefore, the combined units will exhibit angular motions only at the hinge part and keep stiff at each consecutive body of the unit. Since the bending motion will happen at each hinge, the whole structure of either the outer case and the inner chain will generate a compliant bending performance.

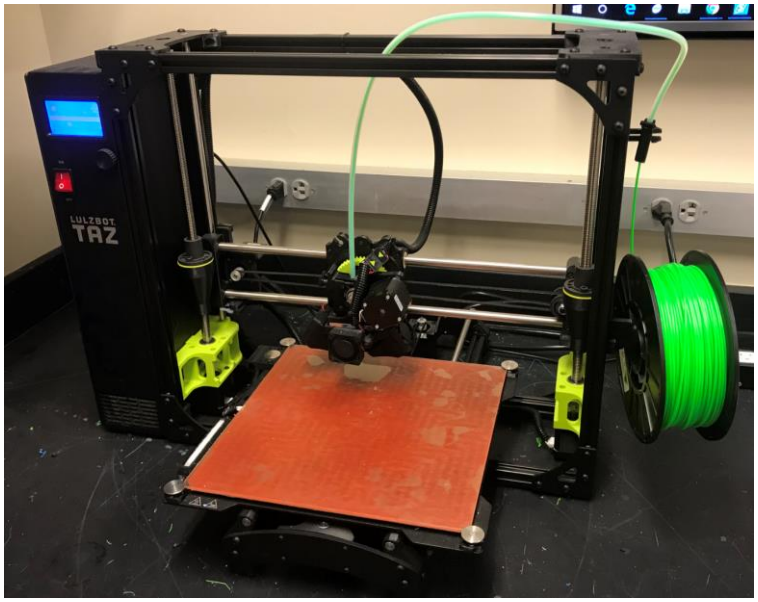

Figure 6.1 3D printer from Gravish's lab, UCSD.

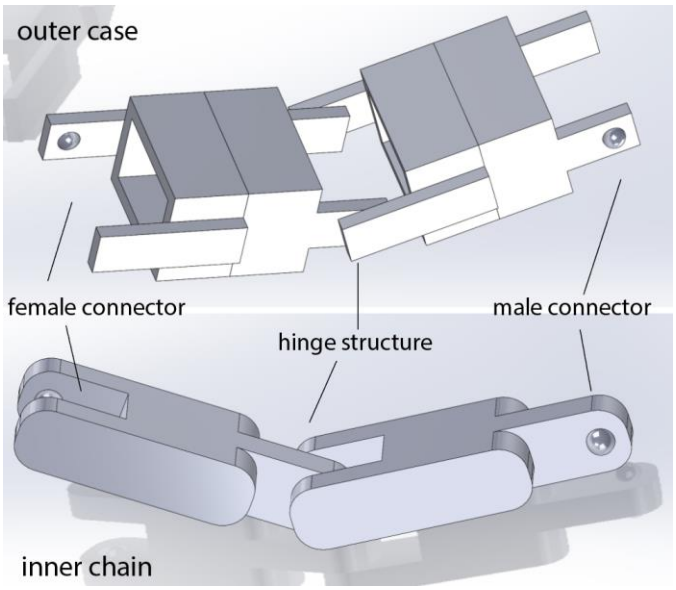

Figure 6.2 3D CAD files showing the conceptual designs of a 3D printed SLL structure. The top figure shows two outer cases connected with a hinge structure and the bottom figure shows two inner chain units linked by a hinge structure which can be slid inside the outer case.

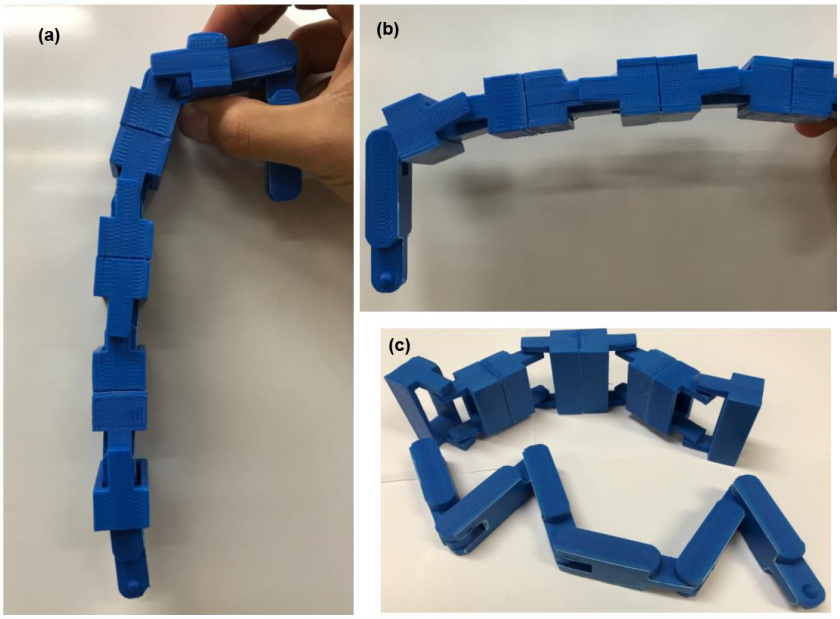

Figure 6.3 3D printed SLL's dual stiffness actuated by the inner chain sliding motion. (a) Soft state 3D printed SLL (b) Stiff state 3D printed SLL, which can hold its only mass (c) Separated inner chain and the outer case using 3D printing technology.

On the other hand, as we slide the inner chain into the outer case to the zero-aligning percentage as we did the laminated SLL, the body of the inner chain unit whose length is longer

than the hinge structure of the outer case will block the angular motion from the outer hinge; in the meanwhile, the outer case, whose length is longer than the hinge structure of the inner chain will block the angular motion from the inner hinge. Since both motions from the hinge are hindered. The whole structure exhibits a strengthened bending stiffness by the blocking effects and is resistive to changing deformations. On the contrary, as we align the hinges from both the outer layer and the inner chain as we did for the laminated SLL (-100%/100% aligning percentage), the whole structure will exhibit different morphological patterns and compliant for external bending moments. Different bending performances are shown in figure 6.3.

Like a laminated SLL, the application of 3D printed SLL can be used to form changing morphologies and bending stiffness which can help manipulating a system's compliance as a structural building block or appendage. With a simplified manufacturing process for variable stiffness structure, a 3D printed SLL can be more favorable in high loads (force, torques) working conditions.

6.2 Ductile SLLs

Ductile SLLs is a laminated material that can change its ductility under certain alignment of a multi-layered laminate. Compared with an elastic SLL, which can modulate stiffness based on the sliding motion of the central laminated layer, a ductile/energy dissipative SLL is fabricated based on ductile materials such as coppers and aluminums. With the central layer consisting by both soft and rigid regions in a periodic pattern, the central layer of a ductile SLL is composed by only rigid and ductile regions with their aligning states correspond to either elastic or ductile/energy dissipative state. Figure 6.4 explains different states of a ductile SLL enabled by layer sliding motion which can form both elastic and ductile performances.

By reconfiguring multiple laminated materials into different aligning states, one can realize a multi-functional material with the ability of modulating one physical property (compliance), or even transitioning between multiple properties (from elastic to ductile). In certain configuration, some properties are explicit, while in other configurations are implicit. Such a changing property enabled by configurable geometrical changes opens a new way to achieve multi-functionalities in future robots.

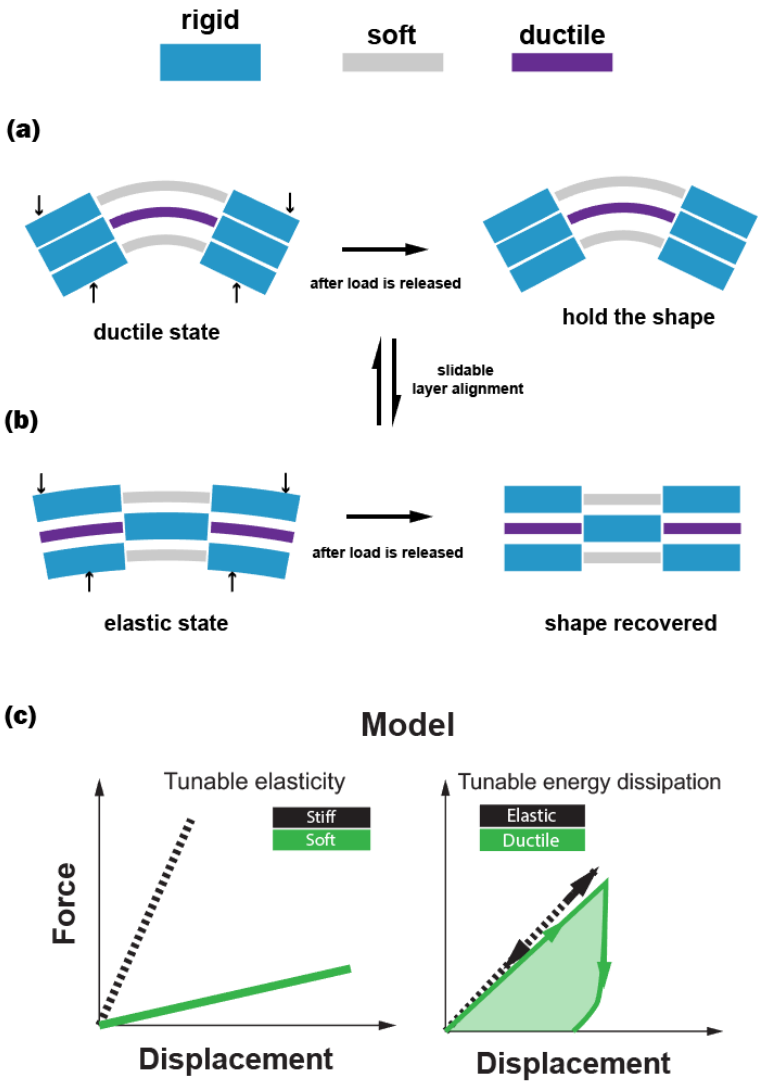

Figure 6.3 Explanations of a ductile SLL's energy dissipative feature (a) Ductile state with energy consumptions and shape holding. (b) Elastic state as a rigid compliance element. (c) A demonstration of the force-displacement curvature between an elastic SLL and a ductile SLL.

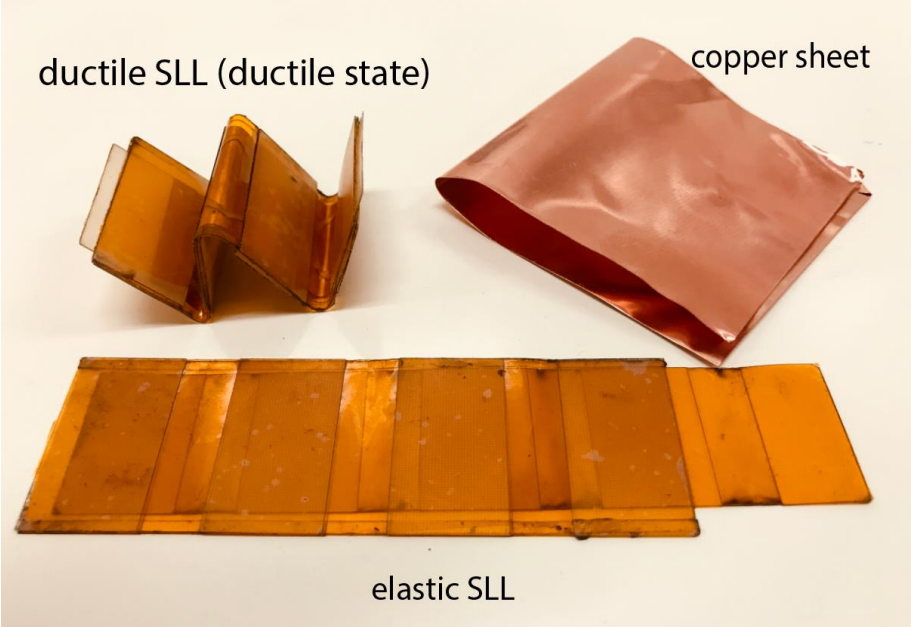

Figure 6.3 a comparison between a ductile SLL and an elastic SLL and their material compositions. The only difference lies in the material composition of the central layers.

6.3 Higher dimensioned SLLs designs

Apart from a SLL prototype fabricated as a laminated strip with only one directional sliding configurations, one can also expand the multi-stiffness laminate into higher dimensions as a suit for different applications and designs. New building blocks such as, a laminated sheet or helical rod or ribbon with individually addressable stiffness or a heterogenous compliance material using multimaterial 3D printing technology will be more applicable in future soft robotics (figure 6.4). Currently, innovative materials such as LCE and SMA are bringing lights for integrated higher dimensioned SLL designs in achieving locally addressable stiffness modulation.

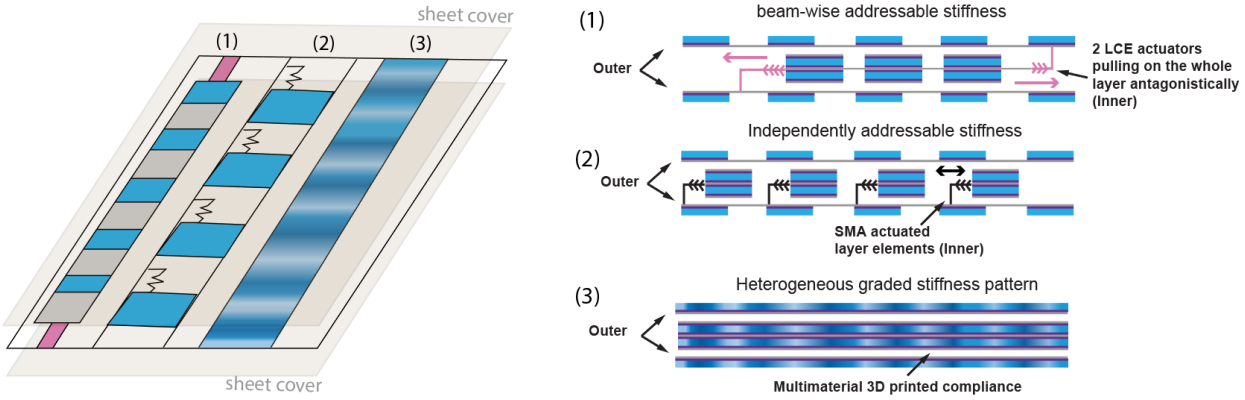

Figure 6.4. Future work in designing SLL in higher dimensions. Left: An integrated smart sheet using SLL concept with high-level design principles: (1) LCE (Liquid Crystal Elastomer) actuators embedded for actuations of the whole layer. (2) Independently addressable stiffness elements enabled by SMA actuators (3) Using multilateral 3D printing techniques to realize heterogenous stiffness pattern.

6.4 Summary

In this chapter, we introduce the extensions of SLL concept into other fields such as 3D printing fabrications, ductile SLLs and higher dimensioned SLL designs. The extensions of SLL concept will help build materials with expanded multi-functionalities enabling a variety of new robotics technologies.

Chapter 7.

Conclusion and Future Work

7.1 Conclusion

In this paper, we present a new material with active stiffness modulation which can enable new types of robots and robotic devices. The conceptual design is based on a dual-stiffness structure analogized by a spring system in both parallel and antagonistic configurations. As we add more layers with periodic stiffness pattern into the system, a multi-layered laminate is created with a sliding mechanism for stiffness modulation, namely a Sliding-Layered-Laminate. As each laminated layer is composed by regions with different flexural rigidities (soft and rigid), the continoutly tunable alignments between each layer will then form different bending stiffness along the longitudinal direction of the whole laminates. Based on Euler-Bernoulli beam theory, we give a formula for stiffness calculation based on the EI profile of each composing layer and predict the stiffness of a long SLL with 100 units under three different design principles, namely, the flexural rigidities of each stiffness region, the aspect ratios of the rigid regions, and the design profiles of the laminated layer, which are based on the reflection of three different perspective of the EI profiles. With different design principles, the stiffness-alignment curvatures are manipulated, bringing changes to the potential range of the stiffness variation as well as different paths for either binary or graded SLLs. In the experiments, we measure the stiffness change of one beam unit under

a series of changing alignments based on two design principles, changing E_rI_r/E_sI_s and changing aspect ratios, which align well with the predicted models. The only discrepancy between the model and the experimental results lies mainly in the SLLs with overall softer bending stiffness, which is expected due to the non-overlapping regions of the stiff state leading to a discontinuous bending curvature that cannot be explained by the model. This exhibits the model's limitations in explaining 3D features (such as laminate gaps) except from the flexural rigidities of the composite laminates. In the demonstration, we first test the fluttering performances in a wind tunnel with a constant air flow speed (2.5m/s), from which we observed changes of compliance with a gradual stiffness modulation by a motorized linear stage. We then implemented the SLL as a robotic fish tail flapping in the water and measured the thrusts generated from its flapping motions as a linearly gliding system constrained by tracks. By tuning the stiffness as well as the driving frequencies, we observed optimized thrusts under different driving frequencies from both soft and stiff state SLL fish tail, indicating that the thrusts of a swimming robot can generate depends on the combination of both driving conditions (sweeping frequencies and amplitudes) and the tail stiffness, which also shows the potential uses of soft state fish tail in a confined aquatic space with a high driving frequency. The tunable stiffness is accomplished using a solenoid with only dual-stiffness change. In the future, an integrated, low-profile actuation methods is desired for continuously tuning of the robotic fish tail's dynamical compliance. In the end, we extend the SLL fabrication process into 3D printing technology and present a chained structure for dual-stiffness materials which consists by only 3D printed materials. However, the applications for SLL is not limited by only compliance, but also other physical properties such as ductility, deformability and viscoelasticity, which broadens the area of multi-functional materials with reconfigurable geometries.

7.2 Future work

As discussed in Chapter 6, the concept for multi-stiffness structure can be broadened into other fields in either innovative manufacturing technologies or higher-dimensioned SLL designs which can be either low-cost in material preparation or with locally addressable stiffness for future robotics applications. In the near future, we are looking forward to implementing such a smart material into practical engineering problems as either a building block or dynamically controlled appendage in the locomotion of flying, swimming and running robots. We believe that a multi-stiffness structure will find its use in achieving the robustness, energy efficiencies and agilities under varying working environments.

Specifically, future applications would be the design of a variable stiffness C-leg using SLL concept for running robots, such as RHex; a variable stiffness fish tail or fin for agile performances of swimming robots; a variable stiffness robotic hinge in a flying robot in modulating resonant frequencies as well as the amplitudes for optimized lifts and thrusts. Figure 7.1 shows the current design of these robots with fixed geometrical structures of their execution appendages.

Therefore, integrating SLL concept into current robotic designs to improve the dynamical performances under changing environments will be favorable in achieving multi-functionalities for future robotics.

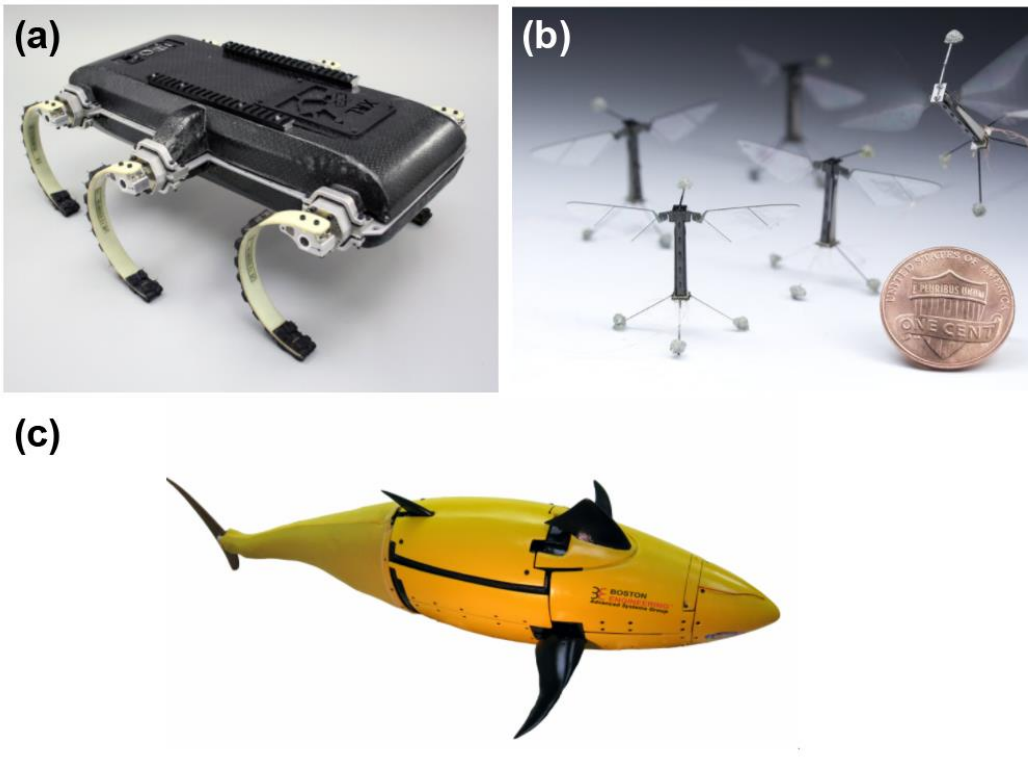

Figure 7.1 current designs for mobile robots (a) RHex (b) RoboBee (c) Robotic Tuna

Bibliography

[1] B. Vanderborght T. Sugar D. Lefeber "Adaptable compliance or variable stiffness for robotic applications" *IEEE Robot. Autom. Mag.* vol. 15 no. 3 pp. 8-9 2008.

[2] G. Mcknight R. Doty A. Keefe G. Herrera C. Henry "Segmented reinforcement variable stiffness materials for reconfigurable surfaces" *J. Intel. Material Syst. Struct.* vol. 21 no. 17 pp. 1783-1793 2010.

[3] Galloway KC, Clark JE, Koditschek DE. Design of a Tunable Stiffness Composite Leg for Dynamic Locomotion. ASME. *International Design Engineering Technical Conferences and Computers and Information in Engineering Conference*, Volume 7: 33rd *Mechanisms and Robotics Conference*, Parts A and B ():215-222. doi:10.1115/DETC2009-86847.

[4] Galloway, K. C., Passive Variable Compliance for Dynamic Legged Robots, PhD thesis, Mechanical Engineering and Applied Mechanics, University of Pennsylvania, Philadelphia, PA (June 2010).

[5] K. Galloway, J. Clark, M. Yim, and D. Koditschek, "Experimental investigations into the role of passive variable compliant legs for dynamic robotic locomotion," in *Robotics and Automation (ICRA), 2011 IEEE International Conference* on, May 2011, pp. 1243–1249.

[6] S. Sponberg and R. J. Full, "Neuromechanical response of musculoskeletal structures in cockroaches during rapid running on rough terrain," *Journal of Experimental Biology*, vol. 211, no. 3, pp. 433– 446, 2008.

[7] Miller BD, Cartes DC, Jonathan E. 2013 Leg stiffness adaptation for running on unknown terrains. In Int. Conf. on Intelligent Robots and Systems (IROS), *2013 IEEE/RSJ*, pp. 5108–5113. IEEE

[8] Maus, H.M., Revzen, S., Guckenheimer, J., Ludwig, C., Reger J. & Seyfarth A. (2015) Constructing predictive models of human running. *R. Soc. Interface*, 12, 20140899.

[9] Park, Y.-J., Huh, T. M., Park, D., and Cho, K.-J. (2014). Design of a variable-stiffness flapping mechanism for maximizing the thrust of a bio-inspired underwater robot. *Bioinspir. Biomim.*9, 36002. doi:10.1088/1748-3182/9/3/036002

[10] Esposito CJ, Tangorra JL, Flammang BE, Lauder GV. 2012 A robotic fish caudal fin: effects of stiffness and motor program on locomotor performance. J. Exp. Biol. 215, 56–67. (doi:10.1242/jeb.062711)

[11] Masataka N., Reiji K., Shunichi K., Hirohisa M., 2009, Bioinspired Propulsion Mechanism Using a Fin with a Dynamic Variable-Effective-Length Spring. J. Biom. Sci. & Eng. Vol. 4, No.1.

[12] M. Manti V. Cacucciolo M. Cianchetti "Stiffening in soft robotics*" IEEE Robot. Autom. Mag.* vol. 23 no. 3 pp. 93-106 Sep. 2016.

[13] Eric Browna, Nicholas Rodenberga, John Amendb, Annan Mozeikac, Erik Steltzc, Mitchell R. Zakind, Hod Lipsonb, and Heinrich M. Jaegera, Universal robotic gripper based on the jamming of granular material. *Proc. Natl Acad. Sci.* USA 107, 18809–18814

[14] S. Follmer, D. Leithinger, A. Olwal, N. Cheng and H. Ishii, "Jamming user interfaces: Programmable particle stiffness and sensing for malleable and shape-changing devices," in *Proc. 25th Annu. ACM Symp. User Interface Software Technology*, 2012, pp. 519–528.

[15] Tolley M T, Felton S M, Miyashita S, Aukes D, Rus D and Wood R J 2014 Self-folding origami: shape memory composites activated by uniform heating. *Smart Mater. Struct.* 23 094006

[16] Felton S, Tolley M, Demaine E, Rus D, Wood R (2014) Applied origami. A method for building self-folding machines. *Science* 345(6197):644–646.

[17] A. J. Loeve, O. S. van de Ven, J. G. Vogel, P. Breedveld, and J. Dankelman, "Vacuum packed particles as flexible endoscope guides with controllable rigidity," *Granular Matter*, vol. 12, no. 6, pp. 543–554, 2010.

[18] Y. J. Kim S. Cheng S. Kim K. Iagnemma "A novel layer jamming mechanism with tunable stiffness capability for minimally invasive surgery" *IEEE Trans. Robot.* vol. 29 no. 4 pp. 1031-1042 2013.

[19] B. Vanderborght, A. Albu-Schaeffer, A. Bicchi, E. Burdet, D. G. Caldwell, R. Carloni, M. Catalano, O. Eiberger, W. Friedl, G. Ganesh, M. Garabini, M. Grebenstein, G. Grioli, S. Haddadin, H. Hoppner, A. Jafari, M. Laffranchi, D. Lefeber, F. Petit, S. Stramigioli, N. Tsagarakis, M. Van Damme, R. Van Ham, L. C. Visser, and S. Wolf, "Variable impedance actuators: A review," Rob. Auton. Syst., vol. 61, no. 12, pp. 1601–1614, 2013.

[20] R. Schiavi G. Grioli S. Sen and A. Bicchi "VSA-II: a novel prototype of variable stiffness actuator for safe and performing robots interacting with humans " *in Proc. IEEE International Conf. on Robotics and Automation (ICRA)* May 2008 p. 2171-2176.

[21] J. Ou L. Yao D. Tauber J. Steimle R. Niiyama H. Ishii "jamsheets: Thin interfaces with tunable stiffness enabled by layer jamming" *Proc. of the 8th Int. Conf. on Tangible Embedded and Embodied Interaction ACM* pp. 65-72 2013.

[22] M. Cianchetti, A. Licofonte, M. Follador, F. Rogai, and C. Laschi, "Bioinspired soft actuation system using shape memory alloys," *Actuators*, vol. 3, no. 3, pp. 226–244, 2014.

[23] A. Hadi Yousefi-KomaA M. Elahinia M. M. Moghaddam and A. Ghazavi. "A shape memory alloy spring-based actuator with stiffness and position controllability". *Proceedings of the Institution of Mechanical Engineers Part I: Journal of Systems and Control Engineering* vol. 225 no. 7 pp. 902-917 2011

[24] C. Majidi R. J. Wood "Tunable elastic stiffness with micro-confined magnetorheological domains at low magnetic field" *Appl. Phys. Lett.* vol. 97 no. 16 pp. 164104 2010.

[25] M. Yuen A. Bilodeau R. Kramer "Active variable stiffness fibers for multifunctional robotic fabrics" *Proc. IEEE Int. Conf. Robot. Autom.* pp. 708-715 May 2016.

[26] H. Imamura, K. Kadooka, M. Taya, A variable stiffness dielectric elastomer actuator based on electrostatic chucking, *Soft Matter*, 13 (2017), pp. 3440-3448

[27] Orita A., Cutkosky M. R., 2016, Scalable electroactive polymer for variable stiffness suspensions, *IEEE/ASME Trans. Mechatronics*, 21 2836–46

[28] W. Shan T. Lu C. Majidi "Soft-matter composites with electrically tunable elastic rigidity" *Smart Mater. Struct*. vol. 22 no. 8 pp. 085005 2013.

[29] R. Pelrine, "Variable stiffness mode: Devices and applications," in *Dielectric Elastomers as Electromechanical Transducers*, F. Carpi, D. De Rossi, R. Kornbluh, R. Pelrine, and P. Sommer Larsen, Eds. New York: Elsevier, 2007, pp. 141–145.

[30] F. Carpi, G. Frediani, C. Gerboni, J. Gemignani, and D. De Rossi, "Enabling variable-stiffness hand rehabilitation orthoses with dielectric elastomer transducers," *Med. Eng. Phys.*, vol. 36, no. 2, pp. 205–211, 2014.

[31] C. Cao and X. Zhao, "Tunable stiffness of electrorheological elastomers by designing mesostructures," *Appl. Phys. Lett*., vol. 103, no. 4, p. 041901, July 2013.

[32] M. Henke, J. Sorber and G. Gerlach, "Multi-layer beam with variable stiffness based on electroactive polymers," in *Proc. SPIE 8340, Electroactive Polymer Actuators and Devices (EAPAD),* 2012, p. 83401P.

[33] K. Singha "A review on coating & lamination in textiles: Processes and applications" *Amer. J. Polymer Sci*. vol. 2 pp. 39-49 2012.

[34] Tolley T M, Felton M S, Miyashita S, Xu L, Shin B-H, Zhou M, Rus D and Wood J R, 2013, Self-folding shape memory laminates for automated fabrication *IEEE/RSJ Int. Conf. on Intelligent Robots and Systems (IROS).*

[35] S. Miyashita L. Meeker M. T. Tolley R. Wood D. Rus "Self-folding miniature elastic electric device" *Smart Mater. Struct.* vol. 23 no. 9 2014.

[36] E. Hawkes B. An N. M. Benbernou H. Tanaka S. Kim E. D. Demaine D. Rus R. J. Wood "Programmable matter by folding" *Proc. Nat. Acad. Sci.* vol. 107--28 pp. 12441-12445 2010.

[37] Y.-J. Park et al. "Dual-stiffness structures with reconfiguring mechanism: Design and investigation" *J. Intell Mater. Sys. Struct. vol.* 27 no. 8 pp. 995-1010 2016.

[38] R. A. A.Campbell, R. W.Eifert and G. C.Turner, "Openstage: a low-cost motorized microscope stage with sub-micron positioning accuracy," *PLoS* One9(2), e88977 (2014).POLNCL1932-6203

[39] G. V. Lauder "Caudal fin locomotion in ray-finned fish: Historical and functional analyses" *Amer. Zool.* vol. 29 pp. 85-102 1989.

[40] M. M. McHenry C. A. Pell J. H. Long Jr. "Mechanical control of swimming speed: Stiffness and axial wave form in undulating fish models" *J. Exp. Biol.* vol. 198 pp. 2293-2305 1995

[41] J. Colgate K. Lynch "Mechanics and control of swimming: A review" *IEEE J. Ocean. Eng.* vol. 29 no. 3 pp. 660-673 Jul. 2004.